

Transverse momentum dependent distributions in dijet and heavy hadron pair production at EIC

Rafael F. del Castillo,^a Miguel G. Echevarria,^{b,c} Yiannis Makris^d and Ignazio Scimemi^a

^a*Dpto. de Física Teórica & IPARCOS, Universidad Complutense de Madrid, E-28040 Madrid, Spain*

^b*Department of Physics, University of the Basque Country UPV/EHU, Apartado 644, 48080 Bilbao, Spain*

^c*University of Alcalá, Dep. of Physics and Mathematics, 28805 Alcalá de Henares (Madrid), Spain*

^d*INFN Sezione di Pavia, via Bassi 6, I-27100 Pavia, Italy*

E-mail: raffer06@ucm.es, miguel.garciae@ehu.eus, yiannis.makris@pv.infn.it,
ignazios@ucm.es

ABSTRACT: We discuss the measurement of gluon transverse momentum distribution (TMD) in dijet and heavy hadron pair (HHP) production in semi-inclusive deep inelastic scattering. The factorization of these processes in position space shows the appearance of a specific new soft factor matrix element on top of angular and complex valued anomalous dimensions. We show in detail how these features can be treated consistently and we discuss a scale prescription for the evolution kernel of the dijet soft function. As a result we obtain phenomenological predictions for unpolarized and angular modulated cross-sections for the electron-ion collider (EIC) using current available information on unpolarized TMD.

Contents

1	Introduction	1
2	Factorization theorem, frame choice and modulations	3
2.1	Notation and kinematics	3
2.2	Factorization theorem for dijet and heavy hadron pair production	4
3	Cross-sections used in phenomenology	6
3.1	Extracting the Born-level cross-sections	7
3.2	Angle integrated and azimuthally modulated cross-section	7
4	Evolution kernels with angular dependent anomalous dimensions	8
4.1	Dijet soft function and angle dependent anomalous dimensions	9
4.2	Treatment of angular dependent anomalous dimensions and resummation	9
5	Evolution kernels and scale choices	15
5.1	ζ -prescription for dijet evolution kernel	16
6	Dijet and heavy hadron pair (HHP) production at EIC	18
6.1	Results	20
6.1.1	Results for dijet production	21
6.1.2	Results for heavy hadron production	23
7	Conclusions	23
A	Hard prefactors	25
B	Anomalous dimensions	26

1 Introduction

The access to non-perturbative gluon distributions from experiments is notoriously challenging. This is also the case of gluon transverse momentum distributions (TMDs). Gluons enter directly in Higgs production in hadronic colliders [1–5] that has a relatively high mass and low production rates, and quarkonium production both at EIC and LHC [3, 6–25] that is sensitive also to the heavy quark hadronization effects [20, 21]. Recent studies (see for example [26, 27]) suggest that the experimental observation of the dijet imbalance is possible at the future EIC. In a recent work [28] we have proposed the dijet and hadron pair production at electron-ion colliders (EIC) to probe gluon TMD. Previous studies on these processes were performed in ref. [29, 30] for dijet and in ref. [31–33] for heavy-meson pair production in an electron-hadron collider. The relevant processes for our case are

$$\ell + h \rightarrow \ell' + J_1 + J_2 + X, \quad \text{and} \quad \ell + h \rightarrow \ell' + H + \bar{H} + X, \quad (1.1)$$

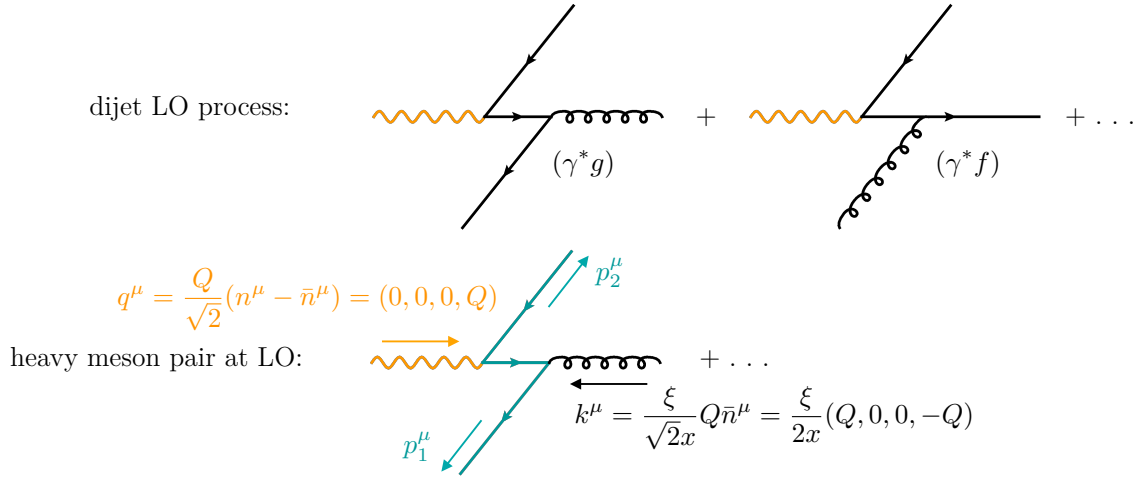


Figure 1: Example LO diagrams for the two processes. The momenta q^μ and k^μ (corresponding to the photon and incoming parton momenta respectively) are expressed in the Breit frame.

where ℓ and ℓ' are the initial and final state leptons, h is the colliding hadron, J_i and H/\bar{H} are the jets and heavy mesons respectively and X represent undetected particles. At leading order (LO), and ignoring the intrinsic momentum of partons inside the target hadron, the two hard-scattering processes are schematically shown in fig. 1. We have shown that these processes are factorizable when considering the cross-section

$$\frac{d\sigma}{dx d\eta_1 d\eta_2 dp_T d\mathbf{r}_T}, \quad (1.2)$$

where x is the Bjorken variable, and η_i , \mathbf{r}_T and p_T are respectively the rapidity, the sum of the transverse momenta (with respect to the beam axis) and the average scalar transverse momenta of the two final jets. The factorization condition is $|\mathbf{r}_T| \ll p_T$ in the Breit frame, as the virtual photon and target-hadron directions are back-to-back. These conditions are certainly fulfilled in the Breit frame for $p_T \in [5, 40]$ GeV and in the central rapidity region. We also demand that there are no hierarchies among partonic Mandelstam variables, $\hat{s} \sim |\hat{t}| \sim |\hat{u}|$. On the experimental side recent studies [26] suggest that the measurement of dijet imbalance is possible at EIC. For the heavy-meson case monte-carlo generator studies suggest that charmed mesons can be reconstructed [34, 35]. The charm production rates have been considered at the LO and NLO QCD for $ep \rightarrow c/\bar{c} + X$ in ref. [36]. For our case in principle we require the transverse momenta of the heavy mesons, $p_T^{H/\bar{H}}$, be parametrically larger than their mass, m_H , i.e. $p_T^{H/\bar{H}} \gg m_H$.

At leading order (LO) the jet processes can be initiated by either a gluon or a quark, while in the heavy-meson case only the gluon initial state is relevant. The factorized cross-section results in products/convolutions of several fundamental functions as TMDs, jet/heavy quark distributions, soft function and a new evolution kernel, detailed in [28]. The purpose of the present paper is to provide a phenomenological study of these processes, including theoretical errors. In order to achieve this, we have used the code Artemide [37], introducing new moduli necessary to describe the present cases. The code already includes quark TMDPDF and the TMD evolution kernel extracted from Drell-Yan and semi-inclusive DIS experiments [38].

The factorization of the cross-section is produced in position space, described by the variable \mathbf{b} , conjugate of the momentum \mathbf{r}_T . In order to Fourier transform the factorized cross-section from \mathbf{b} space to momentum space one has to perform an angular integration on ϕ_b (i.e. $d^2\mathbf{b} = b db d\phi_b$ and $\mathbf{v}_J \cdot \mathbf{b} = v_J b \cos \phi_b$) that results non trivial because the anomalous dimensions of several functions depend on this angle and are complex valued. We show that this integration can be performed in resummed perturbation theory and that this addresses the problem of complex values in all anomalous dimensions. As a result the ϕ_b -angle integrated cross-section is then factorized into distributions that are \mathbf{b} -rotation invariant. The ϕ_b -angle integrated dijet evolution kernel is derived integrating a system of coupled differential equations similar to the TMD case. We show and discuss here a specific scale choice prescription that is analogue to the ζ -prescription already discussed in [39], which was already implemented in Artemide.

The factorization theorem and the detailed definition of the observables is provided in sec. 2. The cross-sections subtleties discovered when comparing to other groups are discussed in sec. 3. The resummation of logs involves angular integrations as explained in sec. 4, which leads to the evolution kernels detailed in sec. 5. The phenomenological results obtained with the codes that we have developed are summarized in sec. 6, after which the conclusions are drawn.

2 Factorization theorem, frame choice and modulations

2.1 Notation and kinematics

In order to define angles and to deduce a factorized cross-section we need to establish some kinematics. The direction of the beam is fixed along the \hat{z} axis. It is useful to define the four-vectors $n^\mu = \frac{1}{\sqrt{2}}(1, 0, 0, 1)$, $\bar{n}^\mu = \frac{1}{\sqrt{2}}(1, 0, 0, -1)$, so that $n^2 = \bar{n}^2 = 0$, $\bar{n} \cdot n = 1$. Then any other four vector can be decomposed into its light-cone components,

$$p^\mu = p_+ \bar{n}^\mu + p_- n^\mu + p_\perp^\mu = (p_+, p_-, p_\perp)_n, \quad (2.1)$$

with

$$p_+ = n \cdot p, \quad p_- = \bar{n} \cdot p, \quad p_\perp^2 = 2p_+ p_- - p^2. \quad (2.2)$$

The direction of the two jets are v_1 and v_2 , normalized as

$$v_J^2 = \bar{v}_J^2 = 0, \quad v_J \cdot \bar{v}_J = 1, \quad \text{with } J = 1, 2, \quad (2.3)$$

and \bar{v}_J are defined by reversing the sign of the spacial components. We have then the standard Lorentz-invariants,

$$Q^2 = -q^2, \quad x = \frac{Q^2}{2P \cdot q}, \quad (2.4)$$

where q^μ is the momentum of the virtual photon, P^μ is the momentum of the target hadron. In the Breit frame we have $q^\mu = (0, 0, 0, Q)$ and neglecting mass corrections $P^\mu = \frac{1}{2x}(Q, 0, 0, -Q)$. The ratio of the longitudinal momenta of the incoming parton and the target hadron is $\xi = \frac{k^+}{P^+}$. with k^μ the momentum of the parton entering hard process. We can then express the variables Q and ξ in terms

of the Born level kinematics using the pseudo-rapidities, η_1 and η_2 , and the transverse momentum, p_T , of the two outgoing partons,

$$Q = 2p_T \cosh(\eta_-) \exp(\eta_+), \quad \xi = 2x \cosh(\eta_+) \exp(-\eta_+), \quad (2.5)$$

where, neglecting corrections from the target hadron mass, $\eta_{\pm} = \frac{\eta_1 \pm \eta_2}{2}$. The partonic Mandelstam variables can be written using the same variables,

$$\begin{aligned} \hat{s} &= (q + k)^2 = 4p_T^2 \cosh^2(\eta_-), \\ \hat{t} &= (q - p_2)^2 = -4p_T^2 \cosh(\eta_-) \cosh(\eta_+) \exp(\eta_1), \\ \hat{u} &= (q - p_1)^2 = -4p_T^2 \cosh(\eta_-) \cosh(\eta_+) \exp(\eta_2), \end{aligned} \quad (2.6)$$

with p_1^μ and p_2^μ the momenta of the outgoing partons. At partonic level they satisfy

$$\hat{s} + \hat{t} + \hat{u} = -Q^2. \quad (2.7)$$

Finally, the transverse momentum imbalance of the two jets, \mathbf{r}_T , and the hard transverse momentum, p_T , are defined through

$$\mathbf{r}_T = \mathbf{p}_{1T} + \mathbf{p}_{2T}, \quad \mathbf{p}_T = \frac{\mathbf{p}_{1T} - \mathbf{p}_{2T}}{2}, \quad (2.8)$$

where the sub-index 1, 2 refers to the final jets. At Born level $\mathbf{p}_{1T} = -\mathbf{p}_{2T}$ and thus $\mathbf{r}_T = 0$. It must be taken into account that the hadronization of the outgoing partons will form jet-like configurations along similar directions and wide angle radiation that can escape the jet clustering algorithm, affecting the imbalance.

2.2 Factorization theorem for dijet and heavy hadron pair production

The factorization of dijet and heavy hadron pair production at leading power (LP) for semi-inclusive deep inelastic experiments has already been provided in [28]. The cross-sections reported here do not take into account any leptonic fiducial cuts, which however could be implemented once the experimental conditions are established (especially at EIC). In this section we recall the main formulas that are used in our phenomenological description. We start with the dijet cross-section which can be written as a sum of terms depending on the parton that initiates the hard process (quark or gluon)

$$d\sigma_{2J} = d\sigma(\gamma^* g) + d\sigma^U(\gamma^* f), \quad (2.9)$$

$$d\sigma(\gamma^* g) = d\sigma^U(\gamma^* g) + d\sigma^L(\gamma^* g). \quad (2.10)$$

For an unpolarized hadronic process, the cross-section is made out of hard contributions from unpolarized initial quarks $d\sigma^U(\gamma^* f)$, unpolarized initial gluons $d\sigma^U(\gamma^* g)$, and linearly polarized gluons $d\sigma^L(\gamma^* g)$. The quark contribution to the cross-section is

$$\begin{aligned} \frac{d\sigma^U(\gamma^* f)}{dx d\eta_1 d\eta_2 dp_T d\mathbf{r}_T} &= \sum_f \sigma_0^{fU} H_{\gamma^* f \rightarrow gf}^U(\hat{s}, \hat{t}, \hat{u}, \mu) \int \frac{d^2\mathbf{b}}{(2\pi)^2} \exp(i\mathbf{b} \cdot \mathbf{r}_T) f_1^f(\xi, \mathbf{b}, \mu, \zeta_1) \\ &\times S_{\gamma f}(\mathbf{b}, \zeta_2, \mu) \left(\mathcal{C}_g(\mathbf{b}, R, \mu) J_g(p_T, R, \mu) \right) \left(\mathcal{C}_f(\mathbf{b}, R, \mu) J_f(p_T, R, \mu) \right). \end{aligned} \quad (2.11)$$

In this formula f_1^f is the unpolarized quark TMDPDF for flavor f , H^U the hard factor for the unpolarized quark case. The perturbative calculations of TMDPDF has been performed recently at NNLO [5, 40–43] and N3LO [44, 45]. The jets are described by the product of a collinear-soft function $\mathcal{C}_{(f,g)}$ and a jet shape function $J_{(f,g)}$ specific for each partonic flavor. The calculation at NLO of these functions can be found in [46, 47] for generic k_T -type and cone jet algorithms.

The factor $S_{\gamma f}$ is the dijet soft function for the fundamental representation of $SU(3)_C$ and calculated in [28] up to NLO. A corresponding soft factor, $S_{\gamma g}$, for the adjoint representation of $SU(3)_C$ is also necessary for the incoming gluon contribution.

$$\begin{aligned} \frac{d\sigma(\gamma^*g)}{dx d\eta_1 d\eta_2 dp_T d\mathbf{r}_T} &= \sum_f H_{\gamma^*g \rightarrow f\bar{f}}^{\mu\nu}(\hat{s}, \hat{t}, \hat{u}, \mu) \int \frac{d^2\mathbf{b}}{(2\pi)^2} \exp(i\mathbf{b} \cdot \mathbf{r}_T) F_{g,\mu\nu}(\xi, \mathbf{b}, \mu, \zeta_1) \\ &\times S_{\gamma g}(\mathbf{b}, \eta_1, \eta_2, \mu, \zeta_2) \left(\mathcal{C}_f(\mathbf{b}, R, \mu) J_f(p_T, R, \mu) \right) \left(\mathcal{C}_{\bar{f}}(\mathbf{b}, R, \mu) J_{\bar{f}}(p_T, R, \mu) \right), \end{aligned} \quad (2.12)$$

The hard factor $H^{\mu\nu}(\mu)$ accounts for contributions of unpolarized and linearly polarized gluons,

$$H_{\gamma^*g \rightarrow f\bar{f}}^{\mu\nu} = \sigma_0^{gU} H_{\gamma^*g \rightarrow f\bar{f}}^U \frac{g_T^{\mu\nu}}{d-2} + \sigma_0^{gL} H_{\gamma^*g \rightarrow f\bar{f}}^L \left(-\frac{g_T^{\mu\nu}}{d-2} + \frac{v_{1T}^\mu v_{2T}^\nu + v_{2T}^\mu v_{1T}^\nu}{2 v_{1T} \cdot v_{2T}} \right). \quad (2.13)$$

The TMD tensor $F_{g,\mu\nu}$ can be also decomposed in terms of unpolarized and linearly polarized parts,

$$F_g^{\mu\nu}(\xi, \mathbf{b}) = f_1^g(\xi, \mathbf{b}) \frac{g_T^{\mu\nu}}{d-2} + h_1^\perp(\xi, \mathbf{b}) \left(\frac{g_T^{\mu\nu}}{d-2} + \frac{b^\mu b^\nu}{\mathbf{b}^2} \right), \quad (2.14)$$

with $g_T^{\mu\nu} = g^{\mu\nu} - n^\mu \bar{n}^\nu - \bar{n}^\mu n^\nu$. The hard factors are evaluated up to NNLO in the unpolarized case in [48, 49] and at LO for the linearly polarized case [50]. In these equations f_1^g and h_1^\perp represent the unpolarized and linearly polarized gluon TMD. Both of them are known perturbatively up to NNLO [5, 41, 43]. Combining eq. (2.10, 2.12, 2.13, 2.14) one obtains

$$\begin{aligned} \frac{d\sigma^U(\gamma^*g)}{dx d\eta_1 d\eta_2 dp_T d\mathbf{r}_T} &= \sigma_0^{gU} \sum_f H_{\gamma^*g \rightarrow f\bar{f}}^U(\hat{s}, \hat{t}, \hat{u}, \mu) \int \frac{d^2\mathbf{b}}{(2\pi)^2} \exp(i\mathbf{b} \cdot \mathbf{r}_T) f_1^g(\xi, \mathbf{b}, \mu, \zeta_1) \\ &\times S_{\gamma g}(\mathbf{b}, \zeta_2, \mu) \left(\mathcal{C}_f(\mathbf{b}, R, \mu) J_f(p_T, R, \mu) \right) \left(\mathcal{C}_{\bar{f}}(\mathbf{b}, R, \mu) J_{\bar{f}}(p_T, R, \mu) \right), \end{aligned} \quad (2.15)$$

$$\begin{aligned} \frac{d\sigma^L(\gamma^*g)}{dx d\eta_1 d\eta_2 dp_T d\mathbf{r}_T} &= \sigma_0^{gL} \sum_f H_{\gamma^*g \rightarrow f\bar{f}}^L(\hat{s}, \hat{t}, \hat{u}, \mu) \int \frac{d^2\mathbf{b}}{(2\pi)^2} \exp(i\mathbf{b} \cdot \mathbf{r}_T) h_1^\perp(\xi, \mathbf{b}, \mu, \zeta_1) \\ &\times \frac{s_b^2 - c_b^2}{2} S_{\gamma g}(\mathbf{b}, \zeta_2, \mu) \left(\mathcal{C}_f(\mathbf{b}, R, \mu) J_f(p_T, R, \mu) \right) \left(\mathcal{C}_{\bar{f}}(\mathbf{b}, R, \mu) J_{\bar{f}}(p_T, R, \mu) \right). \end{aligned} \quad (2.16)$$

We use $s_b = \sin \phi_b$ and $c_b = \cos \phi_b$ for the sine and cosine of the angle ϕ_b between the vectors \mathbf{b} and \mathbf{v}_{1T} , respectively. Each of $d\sigma$ has a hard factor that describes the initiating interaction. The coefficients $\sigma_0^{(f,g),(U,L)}$ are introduced such that the leading order hard functions are normalized to the unity, i.e. $H_{LO}^{U(L)} = 1 + \mathcal{O}(\alpha_s)$.

The case of heavy hadron pair is very similar. The measured imbalance \mathbf{r}_T is

$$\mathbf{r}_T = \mathbf{p}_T^H + \mathbf{p}_T^{\bar{H}}, \quad (2.17)$$

where the superscript H indicates a generic heavy meson and \bar{H} the corresponding anti-particle. The imbalance is measured in the Breit frame and assuming the TMD factorization scaling, i.e.,

$|\mathbf{r}_T| \ll p_T^{H, \bar{H}}$. We also assume that the two heavy mesons are fragmented near the kinematic endpoint and carry most of the energy of the heavy quark coming from the hard process. The cross-section reads

$$\frac{d\sigma(\gamma^*g)}{dx d\eta_H d\eta_{\bar{H}} dp_T d\mathbf{r}_T} = H_{\gamma^*g \rightarrow Q\bar{Q}}^{\mu\nu}(\hat{s}, \hat{t}, \hat{u}, \mu) \int \frac{d\mathbf{b}}{(2\pi)^2} \exp(i\mathbf{b} \cdot \mathbf{r}_T) F_{g, \mu\nu}(\xi, \mathbf{b}, \mu, \zeta_1) \times S_{\gamma g}(\mathbf{b}, \mu, \zeta_2) J_{Q \rightarrow H}(\mathbf{b}, p_T, m_Q, \mu) J_{\bar{Q} \rightarrow \bar{H}}(\mathbf{b}, p_T, m_Q, \mu). \quad (2.18)$$

with η_H and $\eta_{\bar{H}}$ the pseudo-rapidities of the heavy mesons, $J_{Q \rightarrow H}$ the heavy quark jet-functions [51, 52]. The hard, soft, and beam functions are the same as in the dijet case. In the hard function we do not consider corrections due to the quark mass and we define

$$p_T = \frac{|\mathbf{p}_T^H| + |\mathbf{p}_T^{\bar{H}}|}{2}, \quad (2.19)$$

The heavy quark jet functions, $J_{Q \rightarrow H}$, can be partially evaluated in perturbation theory as shown in [28]. We work in the limit $p_T \gg m_H \gg \Lambda_{\text{QCD}}$ and the heavy quark jet function can be re-factorized using bHQET. We also have $r_T \ll p_T$ so that it is possible to find large logs of two parametrically different scales in the fragmentation process,

$$\mu_+ = m_Q, \quad \text{and} \quad \mu_{\mathcal{J}} = m_Q \frac{r_T}{p_T}, \quad (2.20)$$

that need to be resummed to ensure the convergence of the expansion. Following [28] the jet function can be firstly factorized into a short distance matching coefficient and a bHQET matrix element,

$$J_{Q \rightarrow H}(\mathbf{b}, p_T, m_Q, \mu) = H_+(m_Q, \mu) \mathcal{J}_{Q \rightarrow H}\left(\mathbf{b}, \frac{m_Q}{p_T}, \mu\right), \quad (2.21)$$

where the coefficient H_+ is

$$H_+(m_Q, \mu) = |C_+(m_Q, \mu)|^2. \quad (2.22)$$

and the two-dimensional shape function is defined in momentum space as

$$\mathcal{J}_{Q \rightarrow H}(\mathbf{r}) = \frac{1}{2 p_H^- N_C} \sum_X \langle 0 | \delta^{(2)}(\mathbf{r} - i\mathbf{v}(\bar{\mathbf{v}} \cdot \partial)) W_v^\dagger h_{v\beta_+} | XH \rangle \langle XH | \bar{h}_{v,\beta_+} W_v \not{v} | 0 \rangle. \quad (2.23)$$

Notice that \mathbf{v} is a Euclidean, two dimensional, transverse component of the light-like four-vector v^μ pointing along the direction of the boosted heavy meson. In position space $\mathcal{J}_{Q \rightarrow H}$ is obtained by Fourier transformation

$$\mathcal{J}_{Q \rightarrow H}\left(\mathbf{b}, \frac{m_Q}{p_T}, \mu\right) = \int d\mathbf{r} \exp(i\mathbf{b} \cdot \mathbf{r}) \mathcal{J}_{Q \rightarrow H}(\mathbf{r}). \quad (2.24)$$

The one-loop expression for these quantities are calculated in [28].

3 Cross-sections used in phenomenology

The cross-sections presented in previous section are usually partially integrated in phenomenological observables. We discuss here these integrations, which also allow us to relate the normalization of our cross-section with the ones obtained in the literature.

3.1 Extracting the Born-level cross-sections

The tree level cross-sections for the dijet and hadron pair production were considered at tree level in ref. [53]. We start considering the gluon case, from which one can easily deduce also the quark case. The gluon hard contribution to the cross-section is described by

$$\frac{d\sigma(\gamma^*g)}{dx d\eta_1 d\eta_2 d\mathbf{p}_T d\mathbf{r}_T} = \frac{\mathcal{N}}{xs} \left[A_0 + A_1 \cos 2\phi'_p + \dots + B_0 \cos 2\phi'_r + \dots \right], \quad (3.1)$$

and the azimuthal angles (ϕ'_r, ϕ'_p) of vectors $\mathbf{p}_T, \mathbf{r}_T$ are measured with respect to the lepton plane. However, our preferred frame is the one where the ϕ_ℓ angle is measured in the plane defined by \mathbf{p}_T and \mathbf{q}_T , the sum of the lepton momenta, and ϕ_r is the azimuthal angle between \mathbf{r}_T and \mathbf{p}_T . In this frame and integrating over the angle ϕ_ℓ we are left with:

$$\frac{d\sigma(\gamma^*g)}{dx d\eta_1 d\eta_2 d\mathbf{p}_T d\mathbf{r}_T} = 2\pi p_T \frac{\mathcal{N}}{xs} \left[A_0 + B_2 \cos(2\phi_r) \right], \quad (3.2)$$

with the factor 2π coming from ϕ_ℓ integration. The LO expressions are obtained by separating the unpolarized and linearly polarized gluon contributions and Fourier transforming. The unpolarized partonic part has a similar form also for quarks, so that we find

$$\left. \frac{d\sigma^U(\gamma^*g)}{dx d\eta_1 d\eta_2 d\mathbf{p}_T d\mathbf{r}_T} \right|_{\text{LO}} = \sigma_0^{gU} \int \frac{d^2\mathbf{b}}{(2\pi)^2} \exp(i\mathbf{b} \cdot \mathbf{r}_T) f_1^g(\xi, \mathbf{b}) = \sigma_0^{gU} f_1^g(\xi, \mathbf{r}_T), \quad (3.3)$$

$$\left. \frac{d\sigma^U(\gamma^*f)}{dx d\eta_1 d\eta_2 d\mathbf{p}_T d\mathbf{r}_T} \right|_{\text{LO}} = \sigma_0^{fU} \int \frac{d^2\mathbf{b}}{(2\pi)^2} \exp(i\mathbf{b} \cdot \mathbf{r}_T) f_1^f(\xi, \mathbf{b}) = \sigma_0^{fU} f_1^f(\xi, \mathbf{r}_T), \quad (3.4)$$

The same for the linearly polarized gluons gives

$$\begin{aligned} \left. \frac{d\sigma^L(\gamma^*g)}{dx d\eta_1 d\eta_2 d\mathbf{p}_T d\mathbf{r}_T} \right|_{\text{LO}} &= \sigma_0^{gL} \int \frac{d^2\mathbf{b}}{(2\pi)^2} \exp(i\mathbf{r}_T \cdot \mathbf{b}) \frac{\sin^2 \phi_b - \cos^2 \phi_b}{2} h_1^\perp(\xi, \mathbf{b}) . \\ &= -\sigma_0^{gL} \int \frac{b db d\phi_b}{8\pi^2} \exp\left(i r_T b \cos(\phi_b - \phi_r)\right) \cos(2\phi_b) h_1^\perp(\xi, \mathbf{b}) \\ &= \cos(2\phi_r) \sigma_0^{gL} \int \frac{b db}{4\pi} J_2(r_T b) h_1^\perp(\xi, \mathbf{b}) \\ &= -\frac{\cos(2\phi_r)}{2} \sigma_0^{gL} h_1^\perp(\xi, \mathbf{r}_T), \end{aligned} \quad (3.5)$$

where notice that $h_1^\perp(\xi, r_T)$ is not the direct Fourier transform of $h_1^\perp(\xi, b)$ and both functions can be related through eq. (2.20) in [3]. We obtain the $\sigma_0^{(g,f)(U,L)}$ prefactors from the structure functions given in eqs. (3.3, 3.5) in [53] and we list them in appendix A.

3.2 Angle integrated and azimuthally modulated cross-section

The scalar cross-section that we finally consider in the phenomenological studies is obtained by integrating over the ϕ_r angle

$$\frac{d\sigma}{d\Pi dr_T} = r_T \int_{-\pi}^{+\pi} d\phi_r \frac{d\sigma}{d\Pi d\mathbf{r}_T}, \quad (3.6)$$

where $d\Pi = dx d\eta_1 d\eta_2 dp_T$. Because the factorized cross-section is always expressed in position space one can write (here $J_{0,2}$ are Bessel functions)

$$\begin{aligned}
\frac{d\sigma}{d\Pi dr_T} &= r_T \int_{-\pi}^{+\pi} d\phi_r \int \frac{d\mathbf{b}}{(2\pi)^2} \exp \left[i r_T b \cos(\phi_b - \phi_r) \right] \frac{d\tilde{\sigma}(\mathbf{b})}{d\Pi d\mathbf{b}} \\
&= r_T \int_0^\infty \frac{b db}{2\pi} J_0(r_T b) \int_{-\pi}^{+\pi} d\phi_b \frac{d\tilde{\sigma}(\mathbf{b})}{d\Pi d\mathbf{b}} \\
&= r_T \int_0^\infty \frac{b db}{2\pi} J_0(r_T b) \int_{-\pi}^{+\pi} d\phi_b \left[\frac{d\tilde{\sigma}^U(\mathbf{b})}{d\Pi d\mathbf{b}} - \frac{\cos 2\phi_b}{2} \frac{d\tilde{\sigma}^L(\mathbf{b})}{d\Pi d\mathbf{b}} \right], \tag{3.7}
\end{aligned}$$

where $d\sigma^U = d\sigma^U(\gamma^* f) + d\sigma^U(\gamma^* g)$, $d\sigma^L = d\sigma^L(\gamma^* g)$ for the dijet case and $d\sigma^{U,L} = d\sigma^{U,L}(\gamma^* g)$ for the heavy hadron pair case.

In our phenomenological analysis we consider also the azimuthal angle average

$$\langle \cos 2\phi_r \rangle \equiv \left[\int_{-\pi}^{+\pi} d\phi_r \cos 2\phi_r \frac{d\sigma}{d\Pi dr_T} \right] / \frac{d\sigma}{d\Pi dr_T}. \tag{3.8}$$

The denominator is what we have discussed in the previous section, so now we will only focus on the numerator,

$$\begin{aligned}
\int_{-\pi}^{+\pi} d\phi_r \cos 2\phi_r \frac{d\sigma}{d\Pi dr_T} &= r_T \int_{-\pi}^{+\pi} d\phi_r \cos 2\phi_r \int \frac{d\mathbf{b}}{(2\pi)^2} \exp \left[i r_T b \cos(\phi_b - \phi_r) \right] \frac{d\tilde{\sigma}(\mathbf{b})}{d\Pi d\mathbf{b}} \\
&= r_T \int_0^\infty \frac{b db}{2\pi} J_2(r_T b) \int_{-\pi}^{+\pi} d\phi_b \cos 2\phi_b \frac{d\tilde{\sigma}(\mathbf{b})}{d\Pi d\mathbf{b}} \\
&= r_T \int_0^\infty \frac{b db}{2\pi} J_2(r_T b) \int_{-\pi}^{+\pi} d\phi_b \left[\cos 2\phi_b \frac{d\tilde{\sigma}^U(\mathbf{b})}{d\Pi d\mathbf{b}} - \frac{\cos^2 2\phi_b}{2} \frac{d\tilde{\sigma}^L(\mathbf{b})}{d\Pi d\mathbf{b}} \right]. \tag{3.9}
\end{aligned}$$

Eqs. (3.7 - 3.9) show the relation among the final cross-section in momentum space and the factorized cross-sections in position space, where we have distinguished between the unpolarized cross-sections generated by gluons and quarks, $d\tilde{\sigma}^U = d\tilde{\sigma}_g^U + d\tilde{\sigma}_f^U$ and the contribution from linearly polarized gluons $d\tilde{\sigma}^L$.

4 Evolution kernels with angular dependent anomalous dimensions

The anomalous dimensions of soft, collinear-soft and heavy-jets matrix elements are angular dependent and complex valued, and both these features are not common in literature. The angular dependence is parameterized here by the angle ϕ_b . In order to discuss the issue we show in sec. 4.1 the dijet soft function as obtained in [28] and then we extend the conclusions to the other functions that have a similar angular dependent structure. The angular dependence of the anomalous dimension is strictly correlated with the imaginary parts of the cross-section in position space. The treatment of the angular dependence in the evolution has been discussed also in [54–56] which propose an approximate treatment. In sec. 4.2 we perform an original analysis discussing in detail how passing from position space to momentum space in the cross-section allows to obtain a real valued cross-section, including resummation. The proof of this statement is here provided at one-loop, and the same mechanism can be conjectured to work at all orders in perturbation theory.

4.1 Dijet soft function and angle dependent anomalous dimensions

The dijet soft function presents several properties that result particularly interesting. The renormalized soft function is obtained from its bare expression

$$S_{\gamma_i}^{\text{bare}}(\mathbf{b}, \zeta_2) = Z_{\gamma_i}^S(\mathbf{b}, \mu, \zeta_2) S_{\gamma_i}(\mathbf{b}, \mu, \zeta_2), \quad (4.1)$$

where the factor $Z_{\gamma_i}^S$ was calculated in [28]. For our purposes it is sufficient to report expression of the soft function in the $\overline{\text{MS}}$ scheme for the (γ^*g) -channel

$$S_{\gamma_g}(\mathbf{b}, \mu, \zeta_2) = 1 + a_s \left\{ C_F \left[\frac{\pi^2}{3} + 2 \ln^2 \left(\frac{B\mu^2 e^{2\gamma_E}}{-A_{\mathbf{b}}} \right) + 4 \text{Li}_2(1 + A_{\mathbf{b}}) \right] \right. \\ \left. + C_A \left[-2 \ln(B\mu^2 e^{2\gamma_E}) \ln \zeta_2 - \ln^2(-A_{\mathbf{b}}) - \frac{\pi^2}{3} - 2 \text{Li}_2(1 + A_{\mathbf{b}}) \right] \right\} + \mathcal{O}(a_s^2), \quad (4.2)$$

and for the (γ^*f) -channel

$$S_{\gamma_f}(\mathbf{b}, \mu, \zeta_2) = 1 + a_s \left\{ C_A \left[\frac{\pi^2}{6} + \ln^2 \left(\frac{B\mu^2 e^{2\gamma_E}}{-A_{\mathbf{b}}} \right) + 2 \text{Li}_2(1 + A_{\mathbf{b}}) + 2 \ln(B\mu^2 e^{2\gamma_E}) \ln \frac{(n \cdot v_1)(v_2 \cdot \mathbf{b})}{(n \cdot v_2)(v_1 \cdot \mathbf{b})} \right] \right. \\ \left. + C_F \ln(B\mu^2 e^{2\gamma_E}) \left[\ln(B\mu^2 e^{2\gamma_E}) - 2 \ln \zeta_2 + 2 \ln \left(\frac{2(n \cdot v_2)}{(v_1 \cdot v_2)(n \cdot v_2)} \right) + 4 \ln(-i v_1 \cdot \hat{\mathbf{b}}) \right] - C_F \frac{\pi^2}{6} \right\} + \mathcal{O}(a_s^2), \quad (4.3)$$

respectively, where we have $A_{\mathbf{b}} = \frac{(v_1 \cdot v_2)}{2(v_1 \cdot \hat{\mathbf{b}})(v_2 \cdot \hat{\mathbf{b}})}$. The expressions above depend explicitly on the angle ϕ_b and we have used $\hat{\mathbf{b}} = \mathbf{b}/|\mathbf{b}|$. The rapidity scale ζ_2 is responsible for the rapidity evolution of this factor and it is related to the TMD rapidity scale ζ_1 by the consistency constraint

$$\zeta_1 \zeta_2 = \frac{(k^-)^2}{A_n} = \frac{\hat{u} \hat{t}}{\hat{s}}. \quad (4.4)$$

The values of ζ_1 and ζ_2 that minimize hard logs are

$$\zeta_1 = p_T^2, \quad \zeta_2 = 1. \quad (4.5)$$

Despite the fact that the scale ζ_2 is dimensionless there are some formal similarities in the evolution of this soft function and the TMD. The dijet soft function double scale evolution is dictated by

$$\frac{d}{d \ln \mu} S_{\gamma_i}(\mathbf{b}, \zeta, \mu) = \gamma_{S_{\gamma_i}}(\mathbf{b}, \mu, \zeta) S_{\gamma_i}(\mathbf{b}, \zeta, \mu), \quad (4.6)$$

$$\frac{d}{d \ln \zeta} S_{\gamma_i}(\mathbf{b}, \zeta, \mu) = -\mathcal{D}_i(\mu, b) S_{\gamma_i}(\mathbf{b}, \zeta, \mu), \quad (4.7)$$

where i is gluon or quark. The rapidity evolution kernel \mathcal{D}_i is the same as in the TMD case, while for the rest we need a special treatment.

4.2 Treatment of angular dependent anomalous dimensions and resummation

The dijet soft function, the collinear-soft function in dijets and the heavy meson jet function in hadron pair production have, as a common feature, an anomalous dimension that is ϕ_b -dependent and that

can include some imaginary parts. The general structure of the anomalous dimension for these cases is

$$\gamma_i(\mathbf{b}, \mu) = \gamma_{\text{cusp}}[\alpha_s] \left(c_i 2 \ln |\cos \phi_b| - c'_i i\pi \Theta(\phi_b) \right) + \text{other } \phi_b \text{ independent terms} \quad (4.8)$$

where

$$\Theta(\phi_b) = \begin{cases} +1 & : -\pi/2 < \phi_b < \pi/2 \\ -1 & : \text{otherwise} \end{cases} \quad (4.9)$$

and the consistency of anomalous dimensions requires

$$\sum_i c_i = \sum_i c'_i = 0, \quad (4.10)$$

where c_i and c'_i are the color coefficients that multiply the corresponding part of the cusp anomalous dimension. The construction of the evolution kernel involves an integration over the angle ϕ_b and after integration all imaginary parts cancel consistently. Note that this does not mean that one can ignore the imaginary components of the anomalous dimensions or fixed order functions as contributions of imaginary terms yield real contributions to the final result.

In order to show the cancellation of the imaginary part we separate the angular dependent part of the evolution kernel from the rest. For instance for the soft function we have

$$\begin{aligned} S_{\gamma_i}(\mathbf{b}, \mu_f, \zeta_{2,f}) &= \exp \left[\int_P \left(\gamma_{S_{\gamma_i}}(\mathbf{b}, \mu, \zeta_2) d \ln \mu - \mathcal{D}_i(\mu, b) d \ln \zeta_2 \right) \right] S(\mathbf{b}; \mu_0, \zeta_{2,0}) \\ &= \exp \left[\int_P \left(\gamma_{S_{\gamma_i}}^\phi(\phi) d \ln \mu + \bar{\gamma}_{S_{\gamma_i}}(b, \mu, \zeta_2) d \ln \mu - \mathcal{D}_i(\mu, b) d \ln \zeta_2 \right) \right] S_{\gamma_i}(\mathbf{b}, \mu_0, \zeta_{2,0}) \\ &= \exp \left[\int_{\mu_0}^{\mu_f} \left(\gamma_{S_{\gamma_i}}^\phi(\phi) d \ln \mu \right) \right] \exp \left[\int_P \left(\bar{\gamma}_{S_{\gamma_i}}(b, \mu, \zeta_2) d \ln \mu - \mathcal{D}_i(\mu, b) d \ln \zeta_2 \right) \right] S_{\gamma_i}(\mathbf{b}, \mu_0, \zeta_{2,0}) \\ &= \mathcal{R}_{S_{\gamma_i}}^\phi \mathcal{R}_{S_{\gamma_i}} S_{\gamma_i}(\mathbf{b}, \mu_0, \zeta_{2,0}). \end{aligned} \quad (4.11)$$

The evolution factor is so splitted in an angular dependent part and the rest. The splitting is clearly not unique, however this should not affect the final result once the angular integration is performed. We have

$$\frac{d}{d \ln \mu} \mathcal{R}_{S_{\gamma_i}}^\phi = \gamma_S^\phi(\phi) \mathcal{R}_{S_{\gamma_i}}^\phi, \quad \frac{d}{d \ln \zeta} \mathcal{R}_{S_{\gamma_i}}^\phi = 0 \quad (4.12)$$

$$\frac{d}{d \ln \mu} \mathcal{R}_{S_{\gamma_i}} = \bar{\gamma}_S \mathcal{R}_{S_{\gamma_i}}, \quad \frac{d}{d \ln \zeta} \mathcal{R}_{S_{\gamma_i}} = -\mathcal{D}_i \mathcal{R}_{S_{\gamma_i}}, \quad (4.13)$$

A similar splitting is done for all other other angular dependent evolution kernels, for which we have used

$$\gamma_{S_{\gamma_g}}^\phi = \gamma_{\text{cusp}} \left[4C_F \ln |\cos \phi_b| \right], \quad (4.14)$$

$$\gamma_{S_{\gamma_f}}^\phi = \gamma_{\text{cusp}} \left[2(C_F + C_A) \ln |\cos \phi_b| - (C_F - C_A) i\pi \Theta(\phi_b) \right], \quad (4.15)$$

$$\gamma_{\mathcal{C}_g}^\phi = \gamma_{\text{cusp}} C_A \left[-2 \ln |\cos \phi_b| - i\pi \Theta(\phi_b) \right], \quad (4.16)$$

$$\gamma_{\mathcal{C}_f}^\phi = \gamma_{\text{cusp}} C_F \left[-2 \ln |\cos \phi_b| \pm i\pi \Theta(\phi_b) \right], \quad (4.17)$$

$$\gamma_J^\phi = \gamma_{\text{cusp}} C_F \left[-2 \ln |\cos \phi_b| \pm i\pi \Theta(\phi_b) \right], \quad (4.18)$$

where the \pm sign refers to quark and anti-quark jet respectively. The angular independent part of the anomalous dimension is simply obtained from the complete expression of the anomalous dimension

$$\gamma_i = \gamma_i^\phi + \bar{\gamma}_i \quad (4.19)$$

with $i = S_{\gamma g}, S_{\gamma f}, C_g, C_f, J$ for each channel. The complete list of one loop anomalous dimensions can be found in appendix B.

In order to describe the implications of the angle integration we consider here the dijet production case, being the HHP one very similar. The separation of the evolution kernels of all functions in an angular dependent part and the rest allows to write the resummed cross-section in position space as

$$\begin{aligned} d\tilde{\sigma}(\mathbf{b}) &\sim \exp \left[\mathcal{A}(\{\mu_i\}) 2 \ln |\cos \phi_b| - \mathcal{B}(\{\mu_i\}) i\pi \Theta(\phi_b) \right] \mathcal{R}(\{\mu_k\} \rightarrow \mu) \\ &\quad \times \left[1 + \sum_{k \in \{H, F, J, S, C\}} a_s(\mu_k) f_k^{[1]}(b, \cos \phi_b) \right] \\ &= |\cos \phi_b|^{2\mathcal{A}} \left(\cos(\mathcal{B}\pi) - i\Theta(\phi_b) \sin(\mathcal{B}\pi) \right) \mathcal{R}(\{\mu_k\} \rightarrow \mu) \left[1 + \sum_{k \in \{H, F, J, S, C\}} a_s(\mu_k) f_k^{[1]}(b, \cos \phi_b) \right] \end{aligned} \quad (4.20)$$

where we have omitted global scale independent hard factors and non-perturbative contributions that we assume independent of the angle ϕ_b . In this equation we have combined the evolution kernel of the functions that appear in the cross-section in

$$\mathcal{A}(\{\mu_i\}) = \sum_{i \in \{S, C\}} c_i \int_{\mu_i}^{\mu} \gamma_{\text{cusp}}[\alpha_s] d \ln \mu', \quad \mathcal{B}(\{\mu_i\}) = \sum_{i \in \{S, C\}} c'_i \int_{\mu_i}^{\mu} \gamma_{\text{cusp}}[\alpha_s] d \ln \mu' \quad (4.21)$$

which are independent of the factorization scale μ because of eq. (4.10), and an angle independent part $\mathcal{R}(\{\mu_k\} \rightarrow \mu)$. The perturbative parts of all functions that appear in the cross-sections at one loop are collected in the factor $\left[1 + \sum_{k \in \{H, F, J, S, C\}} a_s(\mu_k) f_k^{[1]} \right]$. In eq. (4.20) the imaginary part of the cross-section is proportional to the odd function $\Theta(\phi_b)$. We expect so that this part cancel at all orders in perturbation theory when the ϕ_b the Fourier transform is performed like in eq. (3.7-3.9). In the next subsection we show that this is explicitly the case at one loop.

In order to organize the discussion we firstly consider the case of $d\tilde{\sigma}^U$ and then deduce the necessary modifications to get the Fourier transform of $d\tilde{\sigma}^L$. The angular integration of the cross-section at one loop can always be expressed in terms of the following basic integrals:

$$I_n(\mathcal{A}) \equiv \int_{-\pi}^{+\pi} d\phi_b |\cos \phi_b|^{2\mathcal{A}} \ln^n |\cos \phi_b| \quad (4.22)$$

where

$$\begin{aligned} I_0(\mathcal{A}) &= \frac{2\sqrt{\pi} \Gamma(1/2 + \mathcal{A})}{\Gamma(1 + \mathcal{A})}, \\ I_1(\mathcal{A}) &= \frac{\sqrt{\pi} \Gamma(1/2 + \mathcal{A})}{\Gamma(1 + \mathcal{A})} (H_{\mathcal{A}-1/2} - H_{\mathcal{A}}) \\ I_2(\mathcal{A}) &= \frac{\sqrt{\pi} \Gamma(1/2 + \mathcal{A})}{2\Gamma(1 + \mathcal{A})} \left[(H_{\mathcal{A}-1/2} - H_{\mathcal{A}})^2 + \psi^{(1)}\left(\frac{1}{2} + \mathcal{A}\right) - \psi^{(1)}(1 + \mathcal{A}) \right]. \end{aligned} \quad (4.23)$$

The results on the r.h.s. of eq. (4.23) are defined only for $\mathcal{A} > -1/2$. In order to satisfy this condition for every value of b the scales μ_S and μ_C must be chosen appropriately, which at the current level of precision can be done. Next we show the contribution of each term of $f_k^{[1]}$ to the cross-section:

- *Constant terms:* In this case we consider the leading order term in eq. (4.20) together with all terms in the functions $f_k^{[1]}$ that are $\cos \phi_b$ independent. The integral we need to perform is,

$$I_{\text{const.}}(\mathcal{A}, \mathcal{B}) \equiv \int_{-\pi}^{+\pi} d\phi_b |\cos \phi_b|^{2\mathcal{A}} \left(\cos(\mathcal{B}\pi) - i\Theta(\phi_b) \sin(\mathcal{B}\pi) \right) = I_0(\mathcal{A}) \cos(\mathcal{B}\pi) \quad (4.24)$$

and the imaginary part cancels because of parity.

- *Single logarithmic terms:* In this case we consider terms proportional to $\ln(-i \cos \phi_b)$ that appear in the soft and collinear-soft terms $f_S^{[1]}$ and $f_C^{[1]}$ respectively. The relevant integral that we need to perform is

$$I_{\log}(\mathcal{A}, \mathcal{B}) \equiv \int_{-\pi}^{+\pi} d\phi_b |\cos \phi_b|^{2\mathcal{A}} \left(\cos(\mathcal{B}\pi) - i\Theta(\phi_b) \sin(\mathcal{B}\pi) \right) \ln(-i \cos \phi_b). \quad (4.25)$$

Expanding the logarithm as follows

$$\ln(-i \cos \phi_b) = \ln |\cos \phi_b| - \frac{i\pi}{2} \Theta(\phi_b) \quad (4.26)$$

we can split the main integral into one part proportional to $\cos(\mathcal{B}\pi)$ and a second part proportional to $\sin(\mathcal{B}\pi)$. In terms of the integrals in eq. (4.23) we obtain the real valued result

$$I_{\log}(\mathcal{A}, \mathcal{B}) = I_1(\mathcal{A}) \cos(\mathcal{B}\pi) - \frac{\pi}{2} I_0(\mathcal{A}) \sin(\mathcal{B}\pi). \quad (4.27)$$

- *Logarithmic A_b terms:* In the soft function we observe the presence of terms that involve the following combination,

$$A_b = \frac{(v_1 \cdot v_2)}{2(v_1 \cdot \hat{b})(v_1 \cdot \hat{b})} = -\frac{\hat{s}}{4p_T^2 (\cos \phi_b)^2} \quad (4.28)$$

Particularly this term appears in logarithms and di-logarithms. Here we address the double logarithmic terms, i.e.,

$$\ln^2(-A_b) = \ln^2 \left(\frac{\hat{s}}{4p_T^2} \right) - 4 \ln \left(\frac{\hat{s}}{4p_T^2} \right) \ln |\cos \phi_b| + 4 \ln^2 |\cos \phi_b| \quad (4.29)$$

Integrating over ϕ_b the above we obtain three contributions: a constant term, a single-log and a double-log. Thus we can immediately write,

$$\begin{aligned} I_{\log A}(\mathcal{A}, \mathcal{B}) &\equiv \int_{-\pi}^{+\pi} d\phi_b |\cos \phi_b|^{2\mathcal{A}} \left(\cos(\mathcal{B}\pi) - i\Theta(\phi_b) \sin(\mathcal{B}\pi) \right) \ln^2(-A_b) \\ &= \left[\ln^2 \left(\frac{\hat{s}}{4p_T^2} \right) I_0(\mathcal{A}) - 4 \ln \left(\frac{\hat{s}}{4p_T^2} \right) I_1(\mathcal{A}) + 4 I_2(\mathcal{A}) \right] \cos(\mathcal{B}\pi). \end{aligned} \quad (4.30)$$

- *Double logarithmic terms:* In this case we consider terms proportional to $\ln^2(-i \cos \phi_b)$ that appear in the soft and collinear-soft functions. The relevant integral that we need to perform is

$$I_{\log 2}(\mathcal{A}, \mathcal{B}) \equiv \int_{-\pi}^{+\pi} d\phi_b |\cos \phi_b|^{2\mathcal{A}} \left(\cos(\mathcal{B}\pi) - i\Theta(\phi_b) \sin(\mathcal{B}\pi) \right) \ln^2(-i \cos \phi_b) \quad (4.31)$$

we can then expand the logarithm as follows

$$\ln^2(-i \cos \phi_b) = \ln^2 |\cos \phi_b| - \frac{\pi^2}{4} - i\pi\Theta(\phi_b) \ln |\cos \phi_b| \quad (4.32)$$

then we can expand as before in terms proportional to $\sin(\mathcal{B}\pi)$ and terms proportional to $\cos(\mathcal{B}\pi)$

$$I_{\log 2}(\mathcal{A}, \mathcal{B}) = \left[-\frac{\pi^2}{4} I_0(\mathcal{A}) + I_2(\mathcal{A}) \right] \cos(\mathcal{B}\pi) - \pi I_1(\mathcal{A}) \sin(\mathcal{B}\pi). \quad (4.33)$$

In addition we have poly-logarithmic terms which are proportional to $\text{Li}_2(1 - A_b)$,

$$I_{\text{Li}}(\mathcal{A}, \mathcal{B}, \bar{c}) \equiv \cos(\mathcal{B}\pi) \int_{-\pi}^{+\pi} d\phi_b |\cos \phi_b|^{2\mathcal{A}} \text{Li}_2\left(1 - \frac{1}{\bar{c} \cos^2 \phi_b}\right), \quad (4.34)$$

where

$$\bar{c} \equiv \frac{4p_T^2}{\hat{s}}, \quad 0 < \bar{c} \leq 1, \quad (4.35)$$

and where we have dropped the terms proportional to $\sin(\mathcal{B}\pi)$ since they vanish after integration from parity. We can then use properties of the poly-logarithm in order to express this integral in the following form,

$$I_{\text{Li}}(\mathcal{A}, \mathcal{B}, \bar{c}) = \cos(\mathcal{B}\pi) \left\{ -\frac{1}{2} \left[\left(\ln^2 \bar{c} + \frac{\pi^2}{3} \right) I_0(\mathcal{A}) + 4 \ln \bar{c} I_1(\mathcal{A}) + 4 I_2(\mathcal{A}) \right] \right. \\ \left. + \int_{-\pi}^{+\pi} d\phi_b |\cos \phi_b|^{2\mathcal{A}} \left[\text{Li}_2(\bar{c} \cos^2 \phi_b) + \ln(\bar{c} \cos^2 \phi_b) \ln(1 - \bar{c} \cos^2 \phi_b) \right] \right\} \quad (4.36)$$

We can then expand the poly-logarithms and the $\ln(1 - \bar{c} \cos^2 \phi_b)$ in the region $0 < c \leq 1$. This allows us to perform the integral over ϕ_b and obtain the following,

$$I_{\text{Li}}(\mathcal{A}, \mathcal{B}, \bar{c}) = \cos(\mathcal{B}\pi) \left\{ -\frac{1}{2} \left[\left(\ln^2 \bar{c} + \frac{\pi^2}{3} \right) I_0(\mathcal{A}) + 4 I_1(\mathcal{A}) \ln \bar{c} + 4 I_2(\mathcal{A}) \right] \right. \\ \left. - \sum_{n=1}^{\infty} \frac{\bar{c}^n}{n} \left[\left(\ln \bar{c} - \frac{1}{n} \right) I_0(\mathcal{A} + n) + 2 I_1(\mathcal{A} + n) \right] \right\} \quad (4.37)$$

Although this expression is exact it includes a sum extending to infinity. In numerical applications one can truncate this sum at the desired value to achieve a certain numerical precision. This concludes the discussion of all possible cases that appear in the Fourier transform of the unpolarized cross-section.

The part of the cross-section relative to linearly polarized gluons can be treated similarly. In this case we need to incorporate an additional $\cos 2\phi_b$ term in the integrals but this is the only change since the soft and collinear-soft functions that appear in the two contributions are the same as for the dijet case. Using the trigonometric identity $\cos 2\phi_b = 2 \cos^2 \phi_b - 1$ the integrals for this case can be deduced from the discussion of the unpolarized cross-section by the replacement

$$I_n(\mathcal{A}) \quad \longrightarrow \quad -I_n(\mathcal{A} + 1) + \frac{1}{2} I_n(\mathcal{A}). \quad (4.38)$$

Equivalently for the case of angular modulation in eq. (3.8) the following transformations have to be performed,

$$\begin{aligned} d\tilde{\sigma}^U(\mathbf{b}) &: I_n(\mathcal{A}) \longrightarrow -I_n(\mathcal{A}) + 2I_n(\mathcal{A} + 1) \\ d\tilde{\sigma}^L(\mathbf{b}) &: I_n(\mathcal{A}) \longrightarrow -I_n(\mathcal{A}) + 2I_n(\mathcal{A} + 1) - 2I_n(\mathcal{A} + 2). \end{aligned} \quad (4.39)$$

In all these cases one obtains a cancellation of the imaginary part of the cross-section.

Treating perturbatively the angular integration as discussed in this section leads to write eq. (3.7) for the dijet case as

$$\frac{d\sigma}{d\Pi dr_T} = \frac{d\sigma^U(\gamma^*g)}{d\Pi dr_T} + \frac{d\sigma^U(\gamma^*f)}{d\Pi dr_T} + \frac{d\sigma^L(\gamma^*g)}{d\Pi dr_T}, \quad (4.40)$$

where

$$\begin{aligned} \frac{d\sigma^U(\gamma^*g)}{d\Pi dr_T} &= \sum_f \sigma_0^{gU} H_{\gamma^*g \rightarrow f\bar{f}}^U(\hat{s}, \hat{t}, \hat{u}, \mu = p_T) J_f(p_T, R, \mu_J) J_{\bar{f}}(p_T, R, \mu_J) \\ &\times \int_0^{+\infty} bdb J_0(br_T) f_1^g(\xi, \mathbf{b}) \mathcal{R}_g\left(\left(\{\mu_k\}, \zeta_{1,0}, \zeta_{2,0}\right) \rightarrow (p_T, p_T^2, 1)\right) \hat{\sigma}_g^U(b, R, \{\mu_i\}), \end{aligned} \quad (4.41)$$

$$\begin{aligned} \frac{d\sigma^U(\gamma^*f)}{d\Pi dr_T} &= \sum_{f,\bar{f}} \sigma_0^{fU} H_{\gamma^*f \rightarrow g\bar{f}}^U(\hat{s}, \hat{t}, \hat{u}, \mu = p_T) J_f(p_T, R, \mu_J) J_{\bar{f}}(p_T, R, \mu_J) \\ &\times \int_0^{+\infty} bdb J_0(br_T) f_1^f(\xi, \mathbf{b}) \mathcal{R}_g\left(\left(\{\mu_k\}, \zeta_{1,0}, \zeta_{2,0}\right) \rightarrow (p_T, p_T^2, 1)\right) \hat{\sigma}_f^U(b, R, \{\mu_i\}), \end{aligned} \quad (4.42)$$

$$\begin{aligned} \frac{d\sigma^L(\gamma^*g)}{d\Pi dr_T} &= \sum_f \sigma_0^{gL} H_{\gamma^*g \rightarrow f\bar{f}}^L(\hat{s}, \hat{t}, \hat{u}, \mu = p_T) J_f(p_T, R, \mu_J) J_{\bar{f}}(p_T, R, \mu_J) \\ &\times \int_0^{+\infty} bdb J_0(br_T) h_1^\perp(\xi, \mathbf{b}) \mathcal{R}_g\left(\left(\{\mu_k\}, \zeta_{1,0}, \zeta_{2,0}\right) \rightarrow (p_T, p_T^2, 1)\right) \hat{\sigma}_g^L(b, R, \{\mu_i\}), \end{aligned} \quad (4.43)$$

where $\mathcal{R}_{f,g}$ are products of evolution kernels to be described in the next section, and $\hat{\sigma}_{f,g}^{U,L}$ are the result of ϕ_b angular integration and can be written as

$$\hat{\sigma}_g^U = I_{\text{const.}}^{gU} + a_s(\mu_C) \mathcal{C}_f^U(b, R, \mu_C) + a_s(\mu_C) \mathcal{C}_{\bar{f}}^U(b, R, \mu_C) + a_s(\mu_0) S_{\gamma_g}^U(b, \zeta_2, \mu_0), \quad (4.44)$$

$$\hat{\sigma}_f^U = I_{\text{const.}}^{fU} + a_s(\mu_C) \mathcal{C}_f^U(b, R, \mu_C) + a_s(\mu_C) \mathcal{C}_g^U(b, R, \mu_C) + a_s(\mu_0) S_{\gamma_f}^U(b, \zeta_2, \mu_0), \quad (4.45)$$

$$\hat{\sigma}_g^L = I_{\text{const.}}^{gL} + a_s(\mu_C) \mathcal{C}_f^L(b, R, \mu_C) + a_s(\mu_C) \mathcal{C}_{\bar{f}}^L(b, R, \mu_C) + a_s(\mu_0) S_{\gamma_g}^L(b, \zeta_2, \mu_0). \quad (4.46)$$

The functions \mathcal{C} and S in eq. (4.44-4.46) are the result of the ϕ_b integration in collinear-soft and dijet soft functions. For the heavy meson case we have just contributions from gluon scattering,

$$\frac{d\sigma}{d\Pi dr_T} = \frac{d\sigma^U(\gamma^*g)}{d\Pi dr_T} + \frac{d\sigma^L(\gamma^*g)}{d\Pi dr_T}, \quad (4.47)$$

and we have to change $J_{f,\bar{f}} \rightarrow H_+$ and $\mathcal{C}_f \rightarrow \mathcal{J}_{Q \rightarrow H}$ in eq. (4.41-4.43). In the case of angular modulation the cross-sections can also be written as in eq. (4.40-4.47), with the correct values of the functions $I_{\text{const.}}$, \mathcal{C} and S . The non-perturbative effects are in all cases encoded in the evolution kernels, TMD and jet functions. In the next section we describe how the evolution kernels are defined.

5 Evolution kernels and scale choices

The evolution kernels appearing in eq. (4.40-4.47) are

$$\begin{aligned} \mathcal{R}_g\left(\left(\{\mu_k\}, \zeta_{1,0}, \zeta_{2,0}\right) \rightarrow \left(p_T, p_T^2, 1\right)\right) &= \mathcal{R}_{J_f}(\mu_J \rightarrow p_T)^2 \mathcal{R}_{\mathcal{C}_f}(\mu_C \rightarrow p_T)^2 \\ &\times \mathcal{R}_F^g\left(\left(\mu_0, \zeta_{1,0}\right) \rightarrow \left(p_T, p_T^2\right)\right) \mathcal{R}_S^g\left(\left(\mu_0, \zeta_{2,0}\right) \rightarrow \left(p_T, 1\right)\right), \end{aligned} \quad (5.1)$$

$$\begin{aligned} \mathcal{R}_q\left(\left(\{\mu_k\}, \zeta_{1,0}, \zeta_{2,0}\right) \rightarrow \left(p_T, p_T^2, 1\right)\right) &= \mathcal{R}_{J_f}(\mu_J \rightarrow p_T) \mathcal{R}_{J_g}(\mu_J \rightarrow p_T) \mathcal{R}_{\mathcal{C}_f}(\mu_C \rightarrow p_T) \mathcal{R}_{\mathcal{C}_g}(\mu_C \rightarrow p_T) \\ &\times \mathcal{R}_F^g\left(\left(\mu_0, \zeta_{1,0}\right) \rightarrow \left(p_T, p_T^2\right)\right) \mathcal{R}_S^g\left(\left(\mu_0, \zeta_{2,0}\right) \rightarrow \left(p_T, 1\right)\right), \end{aligned} \quad (5.2)$$

where $\mathcal{R}_{J_{f,g}}$ is a jet function kernel, $\mathcal{R}_{\mathcal{C}_{f,g}}$ is the one of collinear-soft functions, $\mathcal{R}_F^{q,g}$ the one of TMD and finally \mathcal{R}_S^{qg} is the one of the dijet soft function. In the heavy quark case the evolution kernels are parameterized like in eq. (5.1) with the usual changes $J_f \rightarrow H_+$ and $\mathcal{C}_f \rightarrow \mathcal{J}_{Q \rightarrow H}$. The kernels for single-scale evolution have a standard form and a review up to NLL is given in [57],

$$\mathcal{R}_i(\mu_i \rightarrow p_T) = e^{K_i(\mu_i \rightarrow p_T)} \left(\frac{\mu_i}{m_i}\right)^{\omega_i(\mu_i \rightarrow p_T)}, \quad i = \{\mathcal{C}_f, \mathcal{C}_g, J_f, J_g, \mathcal{J}_{Q \rightarrow H}, H_+\} \quad (5.3)$$

where

$$\omega_i(\mu_i \rightarrow p_T) \Big|_{\text{NLL}} = -\frac{\Gamma_i^0}{\beta_0} \left[\ln r + \left(\frac{\Gamma_1}{\Gamma_0} - \frac{\beta_1}{\beta_0}\right) \frac{\alpha_s(\mu_i)}{4\pi} (r-1) \right], \quad (5.4)$$

$$\begin{aligned} K_i(\mu_i \rightarrow p_T) \Big|_{\text{NLL}} &= -\frac{\gamma_i^0}{2\beta_0} \ln r - \frac{2\pi\Gamma_i^0}{(\beta_0)^2} \left[\frac{r-1-r \ln r}{\alpha_s(p_T)} \right. \\ &\quad \left. + \left(\frac{\Gamma_1}{\Gamma_0} - \frac{\beta_1}{\beta_0}\right) \frac{1-r+\ln r}{4\pi} + \frac{\beta_1}{8\pi\beta_0} \ln^2 r \right], \end{aligned} \quad (5.5)$$

with $r = \alpha_s(p_T)/\alpha_s(\mu_i)$ and

$$\begin{aligned} \Gamma_{\mathcal{C}_f}^0 &= -4C_F, \quad \Gamma_{\mathcal{C}_g}^0 = -4C_A, \quad \gamma_{\mathcal{C}_{f/g}}^0 = 0, \quad m_{\mathcal{C}_{f/g}} = \frac{Re^{-\gamma_E}}{b}, \\ \Gamma_{J_f}^0 &= 4C_F, \quad \Gamma_{J_g}^0 = 4C_A, \quad \gamma_{J_f}^0 = 6C_F, \quad \gamma_{J_g}^0 = 2\beta_0, \quad m_{J_{f/g}} = p_T R, \\ \Gamma_{\mathcal{J}}^0 &= -4C_F, \quad \gamma_{\mathcal{J}}^0 = 4C_F, \quad m_{\mathcal{J}} = \frac{m_Q/p_T e^{-\gamma_E}}{b}, \\ \Gamma_+^0 &= 4C_F, \quad \gamma_+^0 = 2C_F, \quad m_+ = m_Q, \end{aligned} \quad (5.6)$$

Initial scales μ_i choice is given in sec. 6. The TMD kernel is considered here in the ζ -prescription described in [39] and implemented in the code Artemide [37] that we use,

$$\mathcal{R}_F^{q,g}(\{\mu_0, \zeta_0\} \rightarrow \{\mu_f, \zeta_f\}) = \left(\frac{\zeta_f}{\zeta_\mu(b, \mu_f)}\right)^{-\mathcal{D}_{q,g}(b, \mu_f)}. \quad (5.7)$$

In the next paragraph we define a ζ -prescription also for the dijet evolution kernel $\mathcal{R}_S^g((\mu_0, \zeta_{2,0}) \rightarrow (p_T, 1))$, which is the only missing part.

5.1 ζ -prescription for dijet evolution kernel

The angular independent kernel of the dijet soft function is obtained as a solution of a coupled system of differential equations, reported in eq. (4.13), that are formally very similar to the TMD ones [58, 59]. The anomalous dimensions are given by

$$\bar{\gamma}_{S_{\gamma g}}(\mu, \zeta) = \gamma_{\text{cusp}} \left[2C_F \ln \left(\frac{\mu^2}{\mu_0^2} \right) - C_A \ln \left(\frac{\zeta}{\zeta_{2,0}^{\gamma g}} \right) \right] + \delta\gamma_S^{\gamma g}, \quad (5.8)$$

$$\bar{\gamma}_{S_{\gamma f}}(\mu, \zeta) = \gamma_{\text{cusp}} \left[(C_F + C_A) \ln \left(\frac{\mu^2}{\mu_0^2} \right) - C_F \ln \left(\frac{\zeta}{\zeta_{2,0}^{\gamma f}} \right) \right] + \delta\gamma_S^{\gamma f}, \quad (5.9)$$

where

$$\mu_0 = \frac{2}{b e^{\gamma_E}}, \quad \zeta_{2,0}^{\gamma g} = \left(\frac{4p_T^2}{\hat{s}} \right)^{\frac{2C_F}{C_A}}, \quad \zeta_{2,0}^{\gamma f} = \left(\frac{4p_T^2}{\hat{s}} \right)^{\frac{C_F+C_A}{C_F}} \left(\frac{\hat{t}}{\hat{u}} \right)^{\frac{C_F-C_A}{C_F}}, \quad (5.10)$$

and $\delta\gamma_S$ are the non-cusp SF anomalous dimension, which is known up to three-loops for the gluon-channel and up to one-loop for the quark-channel and are reported in appendix. The anomalous dimension and the rapidity anomalous dimension (RAD) in eq. (4.6, 4.7) satisfy also

$$-\frac{d}{d \ln \zeta} \bar{\gamma}_{S_{\gamma i}}(\mu, \zeta) = \frac{d}{d \ln \mu} \mathcal{D}_i(\mu, b) = \Gamma_{\text{cusp}}(\mu) \quad (5.11)$$

The evolution for the SF takes the general form

$$\mathcal{R}_S^i(\{\mu_i, \zeta_i\} \rightarrow \{\mu_f, \zeta_f\}) = \exp \left[\int_P \left(\bar{\gamma}_{S_{\gamma i}}(\mu, \zeta) d \ln \mu - \mathcal{D}_i(\mu, b) d \ln \zeta \right) \right] \quad (5.12)$$

with $i = q, g$ and $\{\mu_i, \zeta_i\}$ and $\{\mu_f, \zeta_f\}$ being the initial and final points of factorization and rapidity scales. The integration path P is an arbitrary path in the $\{\mu, \zeta\}$ -plane. Eq. (5.11) ensures that the evolution kernel is path only independent when one knows the complete perturbative expansion of the anomalous dimensions. Since this is not the case the path independence is broken. In order to partially restore the path independence we proceed as in [39] defining a ζ -prescription also for the dijet soft function evolution kernel. The ζ -prescription provides a way to choose the initial scale ζ_i of the evolution kernel as a function of μ and b so that the SF does not depend on the initial scale μ_i . This is done by taking the integration path through a null-evolution line in the $\{\mu, \zeta\}$ -plane and then taking a fixed- μ evolution.

To find the null-evolution line we interpret the pair of differential equations (5.11) as a two-dimensional gradient equation $\nabla F = \mathbf{E}F$, where $\mathbf{E} = (\gamma_S(\mu, \zeta), -\mathcal{D}_S(\mu, b))$. The null-evolution line is then an equipotential line of the field \mathbf{E} . In particular, there is a special null-evolution line that passes through the saddle-point $\{\mu_{\text{saddle}}, \zeta_{\text{saddle}}\}$ of the evolution field. We find that the saddle point is exactly $\mu_{\text{saddle}} = \mu_0$ and $\zeta_{\text{saddle}}^{\gamma i} = \zeta_0^{\gamma i}$. If we parameterize the null-evolution line as $\{\mu, \zeta_\mu(b)\}$, the value of ζ_μ is given by

$$\gamma_{S_{\gamma i}}(\mu, \zeta_\mu(b)) = 2\mathcal{D}_{S_{\gamma i}}(\mu, b) \frac{d \ln \zeta_\mu(b)}{d \ln \mu^2}, \quad (5.13)$$

which is solved perturbatively order by order in α_s . The perturbative solution takes the form

$$\zeta_{\mu, \text{pert}}^{\gamma g}(b) = \left(\frac{\mu}{\mu_0} \right)^{\frac{2C_F}{C_A}} \zeta_0^{\gamma g} e^{v^{\gamma g}(\mu, b)}, \quad (5.14)$$

$$\zeta_{\mu, \text{pert}}^{\gamma f}(b) = \left(\frac{\mu}{\mu_0} \right)^{\frac{C_F+C_A}{C_F}} \zeta_0^{\gamma f} e^{v^{\gamma f}(\mu, b)}, \quad (5.15)$$

where

$$v^{\gamma^i}(\mu, b) = \sum_{n=0}^{\infty} a_s^n(\mu) v_n^{\gamma^i}(\mathbf{L}_\mu), \quad \mathbf{L}_\mu = \ln(B\mu^2 e^{2\gamma_E}), \quad (5.16)$$

$$v_0^{\gamma^g}(\mathbf{L}_\mu) = 0, \quad (5.17)$$

$$v_1^{\gamma^g}(\mathbf{L}_\mu) = \frac{2C_F}{C_A} \left[-\frac{\beta_0}{12} \mathbf{L}_\mu^2 + \frac{\frac{\gamma_2}{2C_F} - d^{(2,0)}}{\Gamma_0} \right], \quad (5.18)$$

$$v_2^{\gamma^g}(\mathbf{L}_\mu) = \frac{2C_F}{C_A} \left[-\frac{\beta_0^2}{24} \mathbf{L}_\mu^3 - \left(\frac{\beta_1}{12} + \frac{\beta_0 \Gamma_1}{12\Gamma_0} \right) \mathbf{L}_\mu^2 + \left(\frac{\beta_0 \frac{\gamma_2}{2C_F}}{2\Gamma_0} - \frac{4\beta_0 d^{(2,0)}}{3\Gamma_0} \right) \mathbf{L}_\mu \right. \\ \left. - \frac{\frac{\gamma_2}{2C_F} \Gamma_1 - d^{(2,0)} \Gamma_1}{\Gamma_0^2} + \frac{\frac{\gamma_3}{2C_F} - d^{(3,0)}}{\Gamma_0} \right], \quad (5.19)$$

$$v_0^{\gamma^f}(\mathbf{L}_\mu) = 0, \quad (5.20)$$

and we are using the following notation

$$\mathcal{D}_i(\mu, b) = C_i \sum_{n=1}^{\infty} a_s^n(\mu) \sum_{k=0}^n \mathbf{L}_\mu^k d^{(n,k)}, \quad \delta\gamma_S(\mu) = \sum_{n=1}^{\infty} a_s^n(\mu) \gamma_n, \quad (5.21)$$

$$\beta(a_s) = -\sum_{n=0}^{\infty} a_s^{n+2} \beta_n, \quad \Gamma_{\text{cusp}}(\mu) = C_i \gamma_{\text{cusp}}(\mu) = C_i \sum_{n=0}^{\infty} a_s^{n+1}(\mu) \Gamma_n, \quad (5.22)$$

with $C_i = C_F, C_A$ for quark and gluon channel respectively. Notice that v_0 vanishes as it is proportional to the LO non-cusp AD, which is zero for the SF. The non-cusp AD is not known beyond LO for the quark-channel.

The RAD is a function of b and therefore has important non-perturbative corrections in the large- b region. These corrections can be implemented as a model. The way to proceed is to solve (5.13) for a generic non-perturbative RAD. The equation is solvable but it is difficult to obtain the cancellation of perturbative logarithms in the small- b region. Following [39] we use the perturbative solution for the small- b region and move to the exact (generic RAD) solution for large- b :

$$\zeta_\mu(b) = \zeta_\mu^{\text{pert}}(b) e^{-b^2/B_{\text{NP}}^2} + \zeta_\mu^{\text{exact}}(b) \left(1 - e^{-b^2/B_{\text{NP}}^2} \right), \quad (5.23)$$

with B_{NP} being the b value where non-perturbative (NP) effects become important ($\sim 2.5 \text{ GeV}^{-1}$). We have already discussed the perturbative solution to eq. (5.13). For the exact solution we find

$$\zeta_{\mu, \text{exact}}^{\gamma^g}(b) = \left(\frac{\mu^2}{\mu_0^2} \right)^{\frac{2C_F}{C_A}} \zeta_0^{\gamma^g} e^{-g^{\gamma^g}(a_s, \mathcal{D}_S)/\mathcal{D}_S}, \quad (5.24)$$

$$\zeta_{\mu, \text{exact}}^{\gamma^f}(b) = \left(\frac{\mu^2}{\mu_0^2} \right)^{\frac{C_F+C_A}{C_F}} \zeta_0^{\gamma^f} e^{-g^{\gamma^f}(a_s, \mathcal{D}_S)/\mathcal{D}_S}, \quad (5.25)$$

where

$$g^{\gamma^i}(a_s, \mathcal{D}_S) = \frac{1}{a_s} \frac{\Gamma_0}{2\beta_0^2} \sum_{n=0}^{\infty} a_s^n g_n^{\gamma^i}(\mathcal{D}_S), \quad (5.26)$$

$$g_0^{\gamma g} = \frac{2C_F}{C_A} [e^{-p} - 1 + p], \quad (5.27)$$

$$g_1^{\gamma g} = \frac{2C_F}{C_A} \left[\frac{\beta_1}{\beta_0} \left(e^{-p} - 1 + p - \frac{p^2}{2} \right) - \frac{\Gamma_1}{\Gamma_0} (e^{-p} - 1 + p) \right], \quad (5.28)$$

$$g_0^{\gamma f} = \frac{C_F + C_A}{C_F} [e^{-p} - 1 + p], \quad (5.29)$$

$$g_1^{\gamma f} = \frac{C_F + C_A}{C_F} \left[\frac{\beta_1}{\beta_0} \left(e^{-p} - 1 + p - \frac{p^2}{2} \right) - \frac{\Gamma_1}{\Gamma_0} (e^{-p} - 1 + p) \right], \quad (5.30)$$

and $p = 2\beta_0 \mathcal{D}_S / \Gamma_0$.

Finally, the evolution kernel that provides the evolution from the null-evolution line and that passes through the saddle-point to the final ζ point is given by

$$\mathcal{R}_S^{q,g}(\{\mu_0, \zeta_0\} \rightarrow \{\mu_f, \zeta_f\}) = \left(\frac{\zeta_f}{\zeta_\mu(b, \mu_f)} \right)^{-\mathcal{D}_{q,g}(b, \mu_f)}, \quad (5.31)$$

and if we consider the evolution from an arbitrary initial scale we take

$$\mathcal{R}_S^i(\{\mu_i, \zeta_i\} \rightarrow \{\mu_f, \zeta_f\}) = \frac{\mathcal{R}_S^i(\{\mu_0, \zeta_0\} \rightarrow \{\mu_f, \zeta_f\})}{\mathcal{R}_S^i(\{\mu_0, \zeta_0\} \rightarrow \{\mu_i, \zeta_i\})}. \quad (5.32)$$

with $i = q, g$. This discussion concludes the analysis of all terms that appear in the factorization theorem and the scale prescription. We are now ready for the implementation in the code Artemide [37].

6 Dijet and heavy hadron pair (HHP) production at EIC

In order to test the phenomenology developed in the previous sections we consider the case of the EIC. In [28] we already studied the coverage of the EIC and we concluded that the most favourable case is given for a value of mass energy for dijet production around $\sqrt{s} = 140$ GeV and central rapidity, $\eta_1 = \eta_2 = 0$. Typical values for jet radii and momenta at EIC are respectively $R \sim 0.7$ and $p_T \sim Q/2 \sim 20$ GeV. In order to simplify the discussion we show plots integrated over Bjorken variable x (the longitudinal fraction of momentum ξ that enters in the TMDPDFs is $\xi \sim 2x$) in the allowed kinematic intervals. For the case of central rapidity we have $x \in (0.0859, 0.5)$. The cross-sections that we plot are

$$\int_{x_{\min}}^{x_{\max}} dx \frac{d\sigma}{dx d\eta_1 d\eta_2 dp_T dr_T} \Big|_{\eta_1, \eta_2, p_T} \quad (6.1)$$

and its value is presented as a function of the small transverse momentum r_T . The cross-sections and the error bands are obtained by using and preparing specific moduli for the code Artemide [37]. In particular we use the TMD and the TMD evolution kernels already coded in Artemide, that come from the fit [38], while the new functions studied in this work are included in this code for the first time. The gluon TMD is not fitted yet, however in Artemide there is a parameterization for it. The code takes into account that the contribution of linearly polarized gluons is highly suppressed because in the the small- b regime the matching of the linearly polarized gluon TMD onto the gluon PDF starts at order α_s^1 and not at order α_s^0 like other distributions. In ref. [5] the cross section obtained in this way with Pythia 8 and current experimental results for the Higgs transverse

momentum spectrum, which are however not very precise. The non-perturbative effects are expected to be important in the high- b region and they should not alter the small- b behavior of this distribution. Notice also that the non-perturbative effects play a role to control the behavior of the distribution around the Landau pole at large- b , which means a further suppression effect at large- b (as we also observe in the case of unpolarized distributions). Summing up, given the current perturbative and non-perturbative knowledge of TMDs, at this stage we prefer not to push for a hypothetical non-perturbative enhancement of the contribution of linearly polarized gluon TMD.

	\mathcal{C}	\mathcal{J}	S		\mathcal{C}	\mathcal{J}
B_{NP}^i (GeV $^{-1}$)	2.5	2.5	2.5	b_{max} (GeV $^{-1}$)	0.5	0.3

Table 1: Values of non-perturbative parameter B_{NP} and b_{max} prescription chosen for collinear-soft function, heavy meson jet function and dijet soft function. Impact of the variation of B_{NP} is shown in fig. 2.

The factorization that we propose in general needs information of the non-perturbative effects in several functions. For the dijet case we have

$$\mathcal{C}(b, R; p_T) = \mathcal{R}_{\mathcal{C}}(b, R; p_T, \mu_{\mathcal{C}}) \mathcal{C}^{\text{pert}}(b, R; \mu_{\mathcal{C}}) f_{\mathcal{C}}^{\text{NP}}(b, R), \quad (6.2)$$

$$S_{\gamma i}(b; p_T, 1) = \mathcal{R}_S(\{\mu_0, \zeta_0\} \rightarrow \{p_T, 1\}) S_{\gamma i}^{\text{pert}}(b; \mu_0, \zeta_0) f_S^{\text{NP}}(b), \quad (6.3)$$

where the functions with suffix *pert* refer to their perturbative part in the $\overline{\text{MS}}$ scheme which is currently known at one loop. Similarly for the HHP case we need

$$\mathcal{J}(b, m_Q/p_T; p_T) = \mathcal{R}_{\mathcal{J}}(b, m_Q/p_T; p_T, \mu_{\mathcal{J}}) \mathcal{J}^{\text{pert}}(b, m_Q/p_T; \mu_{\mathcal{J}}) f_{\mathcal{J}}^{\text{NP}}(b; m_Q). \quad (6.4)$$

The non-perturbative effects are parameterized as

$$f_i^{\text{NP}}(b) = \exp\left(-\frac{b^2}{(B_{\text{NP}}^i)^2}\right), \quad i = \mathcal{C}, \mathcal{J}, S. \quad (6.5)$$

The values of B_{NP}^i define the non-perturbative model and we have tested several combinations as shown in fig. 2. Higher values of B_{NP}^i are more sensitive to the perturbative series in the low transverse momentum spectrum, and in general provide higher values of the observables. In unpolarized TMD cases we have usually that typical values of B_{NP}^i are around 1-3 GeV $^{-1}$ so we have found reasonable to fix their values as in tab. 1.

The factorization scales $\mu_{\mathcal{C}}$ for dijet and $\mu_{\mathcal{J}}$ for HHP are chosen to minimize perturbative logarithms and to not hit the Landau pole of the strong coupling constant,

$$\mu_{\mathcal{C}} = 2e^{-\gamma_E} \left(\frac{1}{b} + \frac{1}{b_{\text{max}}}\right), \quad (6.6)$$

$$\mu_{\mathcal{J}} = \frac{1}{2}e^{-\gamma_E} \left(\frac{1}{b} + \frac{1}{b_{\text{max}}}\right). \quad (6.7)$$

This scale choice deserves some comments. In the dijet case the scale choice does not include the dependence on the jet radius R . Similarly, the mass of the ratio m_Q/p_T does not enter the collinear-soft function and heavy meson jet. In all cases, this means that there is not a complete cancellation of the logarithms of these functions. The reason is that the ϕ_b integration imposes some constraints on

the choice of scales. In fact, the function $\mathcal{A}(\{\mu_i\})$ defined in eq. (4.21), which depends on the initial scale choice for the soft function, collinear-soft function and heavy meson jet, needs to be $\mathcal{A} > -1/2$ in order to have a well defined angular integration. Because of this constraint some scale choices which could be considered like for instance

$$\mu_{\mathcal{C}} = \frac{Re^{-\gamma_E}}{b}, \quad \mu_{\mathcal{J}} = \frac{m_Q/p_T e^{-\gamma_E}}{b}, \quad (6.8)$$

can not be used. As a result in our approach we only partially resum the logs in the collinear-soft function and the heavy meson jet in order to maintain the structure of ζ -prescription and double scale evolution in the soft function that is described in sec. 5. This leads to the initial scales in eq. (6.6, 6.7).

Finally for the dijet soft function we use the b^* -prescription in the same way as for the TMDPDF:

$$\mu_S = \frac{2e^{-\gamma_E}}{b^*}, \quad b^* = \frac{b}{\sqrt{1 + b^2/b_{\max}^2}}. \quad (6.9)$$

Concerning the theoretical errors, the scale variations in collinear-soft and heavy meson jet function are the main source. This is due to the non-cancellation of logs in the functions by the choice of the initial scales. The choice of the values b_{\max} for collinear-soft function and heavy meson jet account for the convergence of our perturbative result. A more consistent way to treat the resummation of these scales is left for a future work, involving the refactorization of these functions.

For functions that do not depend on b the initial scale choice does not require a prescription or NP-model and it is dictated by the cancellation of the logarithms. For the jet function and the H_+ matching coefficient we have

$$\mu_J = p_T R, \quad \mu_+ = m_Q. \quad (6.10)$$

We use a NP-model for the rapidity anomalous dimension that enters the exact solution for the null-evolution ζ_μ line as it is explained in sec. 5. In particular, we use the same model that has been used for TMDPDF in [38]

$$\mathcal{D}_{F,S}^{\text{NP}} = c_0 b b^*, \quad c_0 = 2.5 \cdot 10^{-2}. \quad (6.11)$$

This model dictates how the rapidity anomalous dimension behaves in the large- b region and is used for both dijet soft function and TMDPDF when performing double scale evolution. While a color re-scaling of the non-perturbative models for gluon TMDPDF and gluon channel soft function with respect to their quark analogues is possible, we observe that this change does not have a significant impact on the cross-section and, therefore, we choose to keep the same model for both quarks and gluons.

6.1 Results

In this section we show our results for the differential cross-section for both dijet and heavy hadron pair production processes. Differential cross-sections are shown with error bands coming from scale variation of the different final and initial scales of the functions appearing in our factorization formulas. Scale variation bands are obtained by changing the considered scale by a factor of 2 up and down relative to its central value.

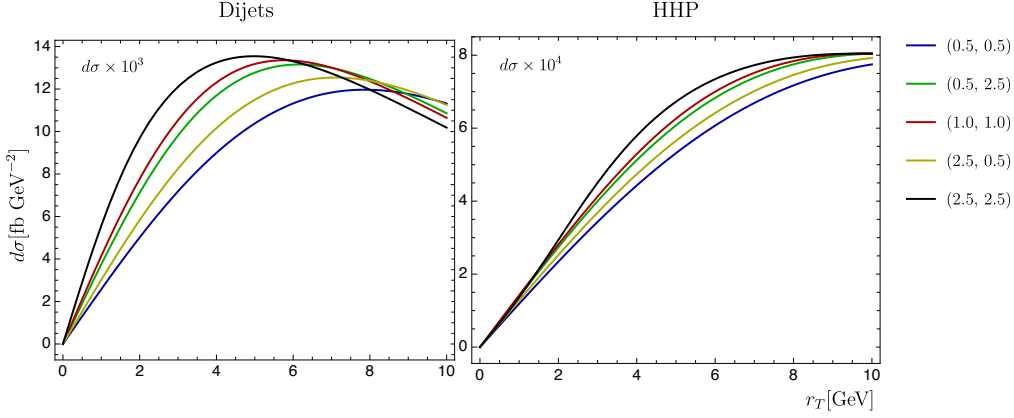


Figure 2: Impact of B_{NP} variation over dijets and heavy meson total cross-section. Legend correspond to $(B_{\text{NP}}^S, B_{\text{NP}}^C)$ and $(B_{\text{NP}}^S, B_{\text{NP}}^J)$ for dijet and HHP production respectively

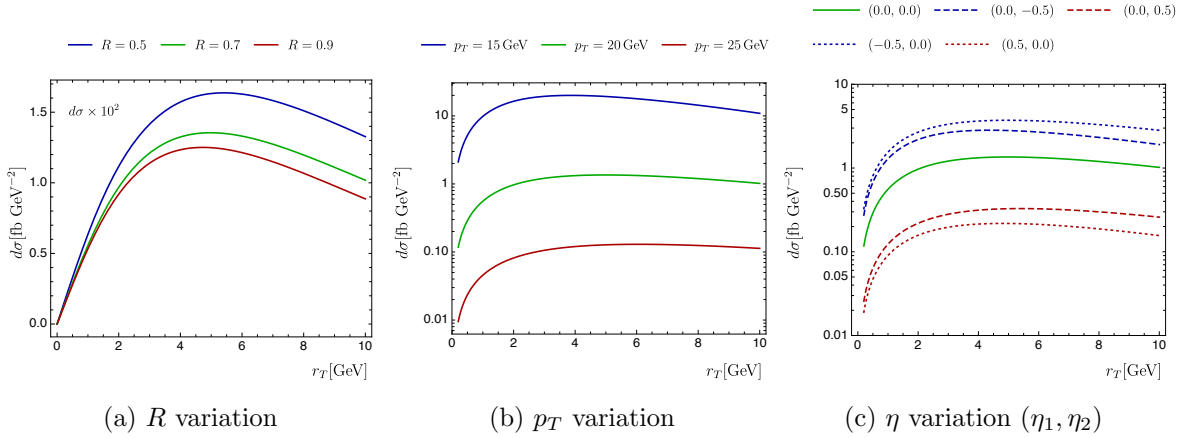


Figure 3: Impact of the variation of the jet radius (R), hard scale jet transverse momentum (p_T) and jet pseudorapidity (η_i) for dijet production. For pseudorapidity variation legend is shown referring to (η_1, η_2) pair, dashed and dotted lines correspond to negative and positive rapidity respectively.

6.1.1 Results for dijet production

In fig. 3 we show the impact of the change of jet radius, jet transverse momentum (hard scale) and jet pseudorapidity over total dijet cross-section. We show that for the variation of the jet radius we see a change of around 20% on the cross-section from the central value when taking the jet radius to be ± 0.2 from $R = 0.7$. For p_T there is a variation of an order of magnitude in the total cross-section when taking ± 5 GeV from 20 GeV. This corresponds to $Q = 30, 40, 50$ GeV respectively. Finally, for pseudorapidity variation we obtain an order of magnitude difference above and below when compared to the central rapidity case. Positive rapidities ($\eta_i = 0.5$) correspond to $Q \simeq 53$ GeV while negative rapidities ($\eta_i = -0.5$) correspond to $Q \simeq 32$ GeV, so both p_T and η plots are consistent. Notice that total dijet cross-section is not symmetrical for both jet rapidities as for quark channel we have both a quark and gluon jet in the final state. Every other plot is obtained taking $R = 0.7$, $p_T = 20$ GeV and $\eta_i = 0$.

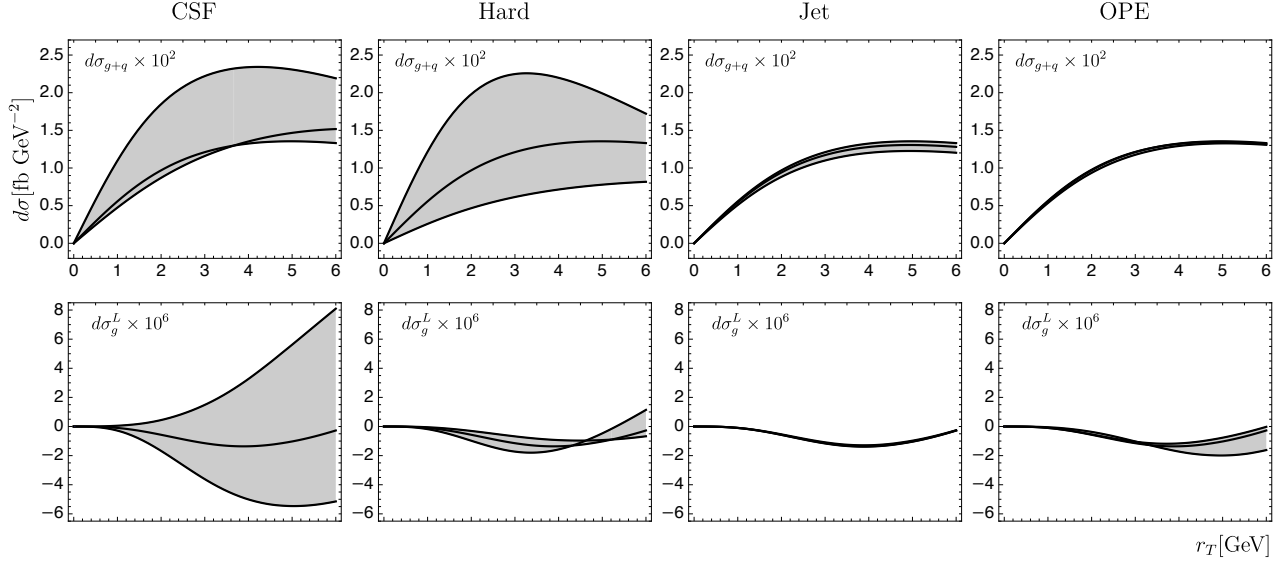


Figure 4: Cross-sections for dijet production at EIC with error-bands coming from scale dependence in collinear-soft factor (CSF), hard factor (Hard), jet distributions (Jet) and Wilson coefficients (OPE). Rows correspond to contributions from linearly polarized gluons (top) and total cross-section (bottom). $\sqrt{s} = 140$ GeV, $R = 0.7$, $p_T = 20$ GeV, $\eta_1 = \eta_2 = 0$.

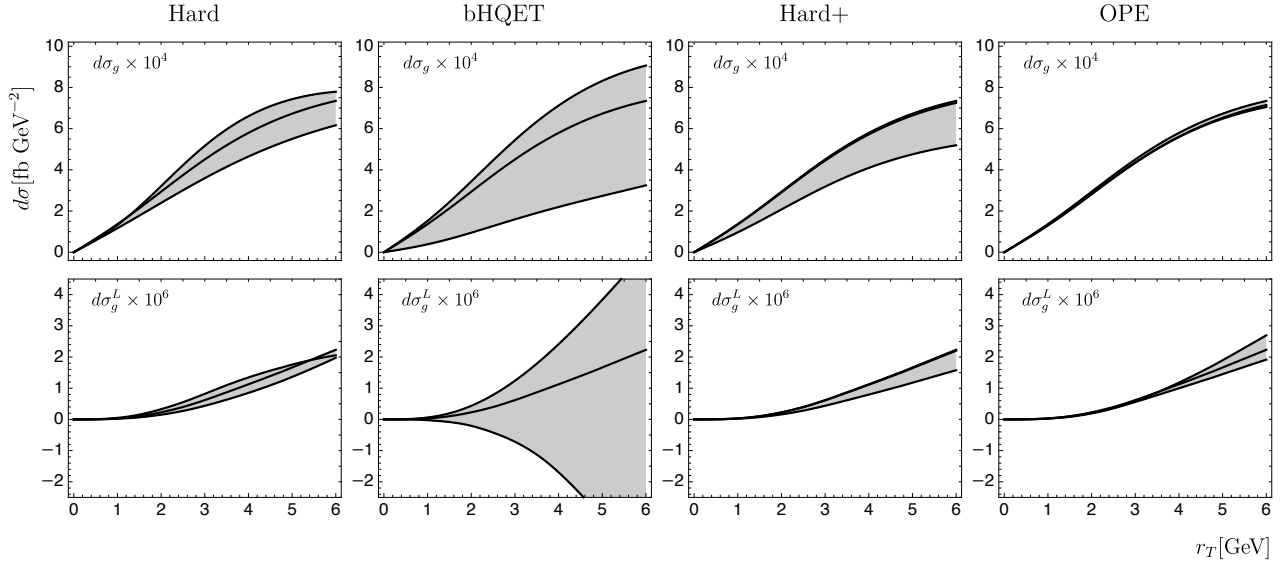


Figure 5: Cross-sections for HHP production at EIC with error-bands coming from scale dependence in hard factor (Hard), heavy meson jet function (bHQET), heavy meson jet function matching coefficient (Hard+) and Wilson coefficients (OPE). The rows correspond to contributions from total cross-section (top) and linearly polarized gluons (bottom). $\sqrt{s} = 140$ GeV, $p_T = 20$ GeV, $\eta_1 = \eta_2 = 0$.

In fig. 4 the result for the cross-section including quark and gluon channels is shown. We consider the contribution of linearly polarized gluons in a separate panel to show that their contribution is com-

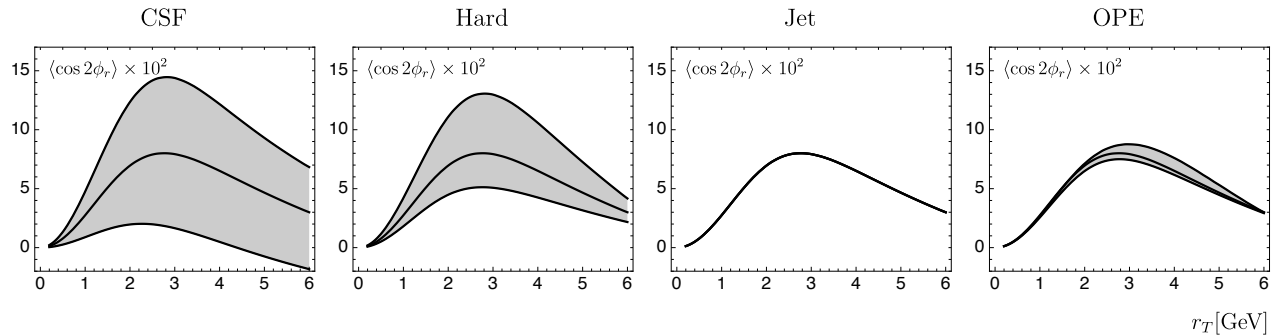


Figure 6: Angular modulation contribution for dijet production at EIC with error-bands coming from scale dependence in collinear-soft factor (CSF), hard factor (Hard), jet distributions (Jet) and Wilson coefficients (OPE). $\sqrt{s} = 140$ GeV, $R = 0.7$, $p_T = 20$ GeV, $\eta_1 = \eta_2 = 0$.

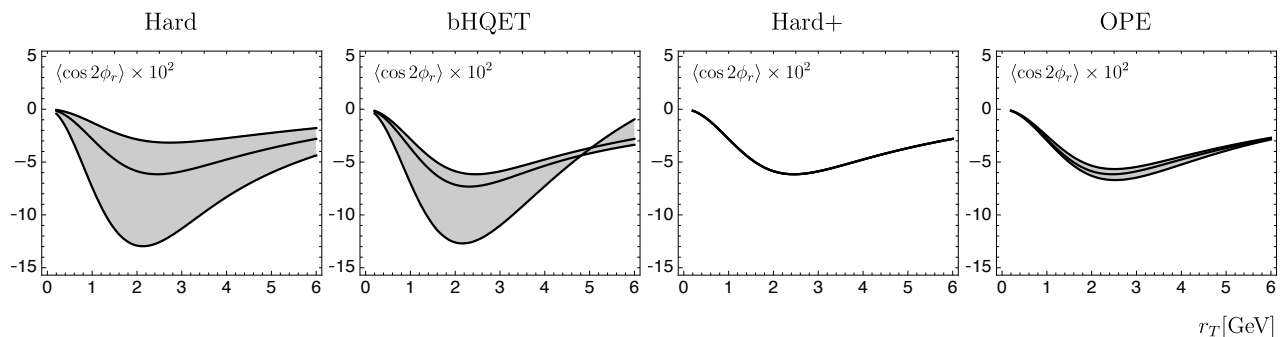


Figure 7: Angular modulation contribution for HHP production at EIC with error-bands coming from scale dependence in hard factor (Hard), heavy meson jet function (bHQET), heavy meson jet function matching coefficient (Hard+) and Wilson coefficients (OPE). $\sqrt{s} = 140$ GeV, $p_T = 20$ GeV, $\eta_1 = \eta_2 = 0$.

pletely negligible, being a factor 10^3 - 10^4 smaller. This leads to the conclusion that the contribution from the linearly polarized gluons can be neglected when considering the unpolarized cross-section.

The angular modulation asymmetry is shown in fig. 6, being around 5%.

6.1.2 Results for heavy hadron production

The analysis for HHP has followed similar steps of the dijet case when possible. The differential cross-section including all channels is plotted in fig. 5. A separate analysis of the contribution of linearly polarized gluons show also in this case that they are completely negligible being suppressed by a factor 10^2 - 10^3 . The angular modulation asymmetry is shown in fig. 7, being around 5%.

7 Conclusions

Dijet and HHP in SIDIS experiments present an opportunity to study the gluon TMD. In this work we have considered the case of the Electron Ion Collider (EIC), as an example. The processes have been proven to factorize consistently and this result has been checked at least at one loop [28]. Nevertheless

the evolution of the functions that appear in the factorization theorem is non-trivial and we propose an original solution, which is generic and independent of the resummation framework. We also note that it is consistent with the ζ -prescription of TMD [39] which we implement in this work. The used prescription allows to separate the evolution kernels from other scale independent factors in the cross-section, so that in our final computations we can use some results already coded in the literature. This is the case for the TMD and their respective evolution kernels extracted from DY and SIDIS data and presented in the code Artemide [37].

The phenomenological analysis that we have performed has revealed several issues that need further study in the future. Estimating the errors due to scale dependence, we have found that several functions need a higher loop calculation to achieve sufficient precision for the low energy jets will be available at EIC. This is the case for instance of the collinear-soft function that appears in the dijet process and more urgently on the heavy hadron jet function. The fact that the perturbative convergence of these function is limited to small values of the b may lead to consider also a re-factorization of these functions, such that the small- b effects are separately resummed. This possibility can eventually be considered in future works.

In all cross-sections we have found a contribution of unpolarized and linearly polarized gluon TMD. For both of these distributions we have used their re-factorization in coefficient functions and collinear PDF studied at higher loops in the literature [5, 41, 43, 45]. In accordance to this well tested procedure, the linearly polarized gluon contribution results to be particularly suppressed in all considered cases, because its matching to collinear PDF starts at order α_s^1 , instead of α_s^0 like the unpolarized distributions. The effect of this suppression is particularly evident in the estimate of the angular modulation of $\cos 2\phi_r$ asymmetry that is here estimated to be around 5%. The study of next-to-leading power effects is beyond the purpose of the present work, so that further study is necessary to confirm a value of this asymmetry.

A source of uncertainty in our prediction comes from the usage of models for many functions that have not been yet compared against data. In this case we have studied several possibilities with simple Gaussian models, assigning values to the non-perturbative parameters according to an educated-guess. The models do not alter the overall-conclusions about scale choices or precision, but can have some effect on the shape of the curves that we have computed. Only an strict comparison with data or eventual lattice calculations can finally resolve this issue.

As a result of this study we can see that the extraction of gluon TMDs from dijet and HHP processes at the EIC is conditioned yet by the possible theoretical and experimental precision. In particular, the linearly polarized gluon TMD appears generally too suppressed and hardly accessible if one uses the usual matching of TMDs onto their collinear counterpart distributions. Nevertheless, the discussed theoretical issues can potentially be solved or improved in future studies.

Acknowledgements

R.F.C., M.G.E. and I.S. are supported by the Spanish Ministry grant PID2019-106080GB-C21. This project has received funding from the European Union Horizon 2020 research and innovation program under grant agreement Num. 824093 (STRONG-2020). M.G.E. is supported by the Community of Madrid and UAH joint grant CM/BG/2021-002 (MultiNuS) within the agreement to fund *Beatriz Galindo* researchers. Y.M. is supported by the European Union's Horizon 2020 research and innovation program under the Marie Skłodowska-Curie grant agreement No. 754496-FELLINI.

A Hard prefactors

The hard prefactors for each channel are given in ref. [53]. We include in this section the ones relevant for our cases

$$\sigma_0^{gU} = 2\pi p_T \frac{\mathcal{N}}{xs} \frac{A_0^{gU}}{f_1^g(\xi, \mathbf{r}_T)}, \quad \sigma_0^{fU} = 2\pi p_T \frac{\mathcal{N}}{xs} \frac{A_0^{fU}}{f_1^f(\xi, \mathbf{r}_T)}, \quad \sigma_0^{gL} = -4\pi p_T \frac{\mathcal{N}}{xs} \frac{B_2}{h_1^\perp(\xi, \mathbf{r}_T)}, \quad (\text{A.1})$$

where

$$\mathcal{N} = \frac{\alpha^2 \alpha_s}{\pi s p_T^2} \frac{1}{xy^2}, \quad (\text{A.2})$$

$$A_0^{gU} = e_q^2 T_R \left[\left(1 + (1 - y^2) \right) A_{U+L}^{gU} - y^2 A_L^{gU} \right] f_1^g(\xi, \mathbf{r}_T), \quad (\text{A.3})$$

$$A_0^{fU} = e_q^2 C_F \left[\left(1 + (1 - y^2) \right) A_{U+L}^{fU} - y^2 A_L^{fU} \right] f_1^q(\xi, \mathbf{r}_T), \quad (\text{A.4})$$

$$B_2 = e_q^2 T_R \left[\left(1 + (1 - y^2) \right) B_{U+L} - y^2 B_L \right] \frac{r_T^2}{M_p^2} h_1^{\perp g}(\xi, \mathbf{r}_T), \quad (\text{A.5})$$

and A and B factors are given by

$$A_{U+L}^{fU} = \frac{1-z}{D^2} \left\{ 1 + z^2 + [2z(1-z) + 4z^2(1-z)^2] \frac{Q^2}{p_T^2} + [z^2(1-z)^2] [1 + (1-z)^2] \frac{Q^4}{p_T^4} \right\}, \quad (\text{A.6})$$

$$A_{U+L}^{gU} = \frac{1}{D^3} - \frac{z(1-z)}{D^3} \left\{ 2 - 8z(1-z) \frac{Q^2}{p_T^2} - z(1-z)[1 - 2z(1-z)] \frac{Q^4}{p_T^4} \right\}, \quad (\text{A.7})$$

$$B_{U+L} = \frac{z(1-z)}{D^3} \left\{ [1 - 6z(1-z)] \frac{Q^2}{p_T^2} \right\}, \quad (\text{A.8})$$

$$A_L^{fU} = 4 \frac{z^2(1-z)^3}{D^2} \frac{Q^2}{p_T^2}, \quad (\text{A.9})$$

$$A_L^{gU} = 8 \frac{z^2(1-z)^2}{D^3} \frac{Q^2}{p_T^2}, \quad (\text{A.10})$$

$$B_L = -4 \frac{z^2(1-z)^2}{D^3} \frac{Q^2}{p_T^2}, \quad (\text{A.11})$$

where D is defined as

$$D = 1 + z(1-z) \frac{Q^2}{p_T^2}. \quad (\text{A.12})$$

B Anomalous dimensions

For the two channels in the dijet process the relevant anomalous dimensions up to one-loop are,

$$\begin{aligned}
\gamma_{H\gamma_g}^{[1]} &= 4\left\{C_F\left[\ln\left(\frac{\hat{s}^2}{\mu^4}\right) - 2\gamma_q\right] + C_A\ln\left(\frac{\hat{t}\hat{u}}{\hat{s}\mu^2}\right)\right\}, \\
\gamma_{H\gamma_f}^{[1]} &= 4\left\{C_F\left[\ln\left(\frac{\hat{u}^2}{\mu^4}\right) - 2\gamma_q\right] + C_A\ln\left(\frac{\hat{s}\hat{t}}{\hat{u}\mu^2}\right)\right\}, \\
\gamma_{S\gamma_g}^{[1]} &= 4\left\{-C_A\ln\zeta_2 + 2C_F\left[\ln(B\mu^2 e^{2\gamma_E}) - \ln\hat{s} + \ln p_T^2 + \ln(4c_b^2)\right]\right\}, \\
\gamma_{S\gamma_f}^{[1]} &= 4\left\{(C_F + C_A)\left[\ln(B\mu^2 e^{2\gamma_E}) - \ln\hat{s} + \ln p_T^2 + \ln(4c_b^2)\right] + (C_F - C_A)\left[\ln\left(\frac{\hat{t}}{\hat{u}}\right) - \kappa(v_f)\right] - C_F\ln\zeta_2\right\} \\
\gamma_{F_i}^{[1]} &= 4C_i\left[-\ln\left(\frac{\zeta_1}{\mu^2}\right) + \gamma_i\right], \\
\gamma_{J_i}^{[1]} &= 4C_i\left[-\ln\left(\frac{p_T^2}{\mu^2}\right) - \ln R^2 + \gamma_i\right], \\
\gamma_{C_g}^{[1]} &= 4C_A\left[-\ln\left(B\mu^2 e^{2\gamma_E}\right) + \ln R^2 - \ln(4c_b^2) + \kappa(v_g)\right], \\
\gamma_{C_i}^{[1]} &= 4C_F\left[-\ln\left(B\mu^2 e^{2\gamma_E}\right) + \ln R^2 - \ln(4c_b^2) + \kappa(v_i)\right], \\
\gamma_{\alpha}^{[1]} &= -4C_A\gamma_g, \tag{B.1}
\end{aligned}$$

The imaginary component in the soft and collinear-soft anomalous dimension is denoted by $\kappa(v_i)$ where

$$\kappa(v_f) = -\kappa(v_{\bar{f}}) = -\kappa(v_g) = i\pi \operatorname{sign}(c_b). \tag{B.2}$$

These anomalous dimensions, except the soft function which we calculated here, can be found in [46–50, 60]. We also expand A_b in the soft function anomalous dimension in terms of \hat{s} , p_T , and c_b . It is now easy to confirm the cancelation of the anomalous dimensions at $\mathcal{O}(\alpha_s)$ which also serves as confirmation of the factorization theorem at the same order.

For the heavy hadron pair case the one-loop hard function, H_+ is,

$$H_+(m_Q, \mu) = 1 + \frac{\alpha_s}{4\pi} C_F \left\{ \ln\left(\frac{\mu^2}{m_Q^2}\right) + \ln^2\left(\frac{\mu^2}{m_Q^2}\right) + 8 + \frac{\pi^2}{6} \right\}, \tag{B.3}$$

and the corresponding anomalous dimension is

$$\gamma_+ = \frac{\alpha_s C_F}{\pi} \left\{ \frac{1}{2} - \ln\left(\frac{m_Q^2}{\mu^2}\right) \right\}. \tag{B.4}$$

The heavy jet functions anomalous dimension is

$$\gamma_{\mathcal{J}} = \frac{\alpha_s C_F}{\pi} \left\{ 1 - 2 \ln \mathcal{R} \right\} \tag{B.5}$$

where

$$\mathcal{R} = -\frac{i p_T \mu e^{\gamma_E} (\mathbf{v} \cdot \mathbf{b})}{m_Q |\mathbf{v}|}. \tag{B.6}$$

References

- [1] Y. Gao, C. S. Li and J. J. Liu, *Transverse momentum resummation for Higgs production in soft-collinear effective theory*, *Phys. Rev. D* **72** (2005) 114020, [[hep-ph/0501229](#)].
- [2] J.-Y. Chiu, A. Jain, D. Neill and I. Z. Rothstein, *A Formalism for the Systematic Treatment of Rapidity Logarithms in Quantum Field Theory*, *JHEP* **05** (2012) 084, [[1202.0814](#)].
- [3] M. G. Echevarria, T. Kasemets, P. J. Mulders and C. Pisano, *QCD evolution of (un)polarized gluon TMDPDFs and the Higgs q_T -distribution*, *JHEP* **07** (2015) 158, [[1502.05354](#)].
- [4] D. Neill, I. Z. Rothstein and V. Vaidya, *The Higgs Transverse Momentum Distribution at NNLL and its Theoretical Errors*, *JHEP* **12** (2015) 097, [[1503.00005](#)].
- [5] D. Gutierrez-Reyes, S. Leal-Gomez, I. Scimemi and A. Vladimirov, *Linearly polarized gluons at next-to-next-to leading order and the Higgs transverse momentum distribution*, *JHEP* **11** (2019) 121, [[1907.03780](#)].
- [6] P. Mulders and J. Rodrigues, *Transverse momentum dependence in gluon distribution and fragmentation functions*, *Phys. Rev. D* **63** (2001) 094021, [[hep-ph/0009343](#)].
- [7] D. Boer and C. Pisano, *Polarized gluon studies with charmonium and bottomonium at LHCb and AFTER*, *Phys. Rev. D* **86** (2012) 094007, [[1208.3642](#)].
- [8] J. Ma, J. Wang and S. Zhao, *Transverse momentum dependent factorization for quarkonium production at low transverse momentum*, *Phys. Rev. D* **88** (2013) 014027, [[1211.7144](#)].
- [9] G.-P. Zhang, *Probing transverse momentum dependent gluon distribution functions from hadronic quarkonium pair production*, *Phys. Rev. D* **90** (2014) 094011, [[1406.5476](#)].
- [10] J. Ma and C. Wang, *QCD factorization for quarkonium production in hadron collisions at low transverse momentum*, *Phys. Rev. D* **93** (2016) 014025, [[1509.04421](#)].
- [11] D. Boer, *Linearly polarized gluon effects in unpolarized collisions*, *PoS QCDEV2015* (2015) 023, [[1510.05915](#)].
- [12] R. Bain, Y. Makris and T. Mehen, *Transverse Momentum Dependent Fragmenting Jet Functions with Applications to Quarkonium Production*, *JHEP* **11** (2016) 144, [[1610.06508](#)].
- [13] A. Mukherjee and S. Rajesh, *Probing Transverse Momentum Dependent Parton Distributions in Charmonium and Bottomonium Production*, *Phys. Rev. D* **93** (2016) 054018, [[1511.04319](#)].
- [14] A. Mukherjee and S. Rajesh, *Linearly polarized gluons in charmonium and bottomonium production in color octet model*, *Phys. Rev. D* **95** (2017) 034039, [[1611.05974](#)].
- [15] J.-P. Lansberg, C. Pisano and M. Schlegel, *Associated production of a dilepton and a $\Upsilon(J/\psi)$ at the LHC as a probe of gluon transverse momentum dependent distributions*, *Nucl. Phys. B* **920** (2017) 192–210, [[1702.00305](#)].
- [16] J.-P. Lansberg, C. Pisano, F. Scarpa and M. Schlegel, *Pinning down the linearly-polarised gluons inside unpolarised protons using quarkonium-pair production at the LHC*, *Phys. Lett. B* **784** (2018) 217–222, [[1710.01684](#)].
- [17] A. Bacchetta, D. Boer, C. Pisano and P. Tael, *Gluon TMDs and NRQCD matrix elements in J/ψ production at an EIC*, *Eur. Phys. J. C* **80** (2020) 72, [[1809.02056](#)].
- [18] C. Hadjidakis et al., *A Fixed-Target Programme at the LHC: Physics Case and Projected Performances for Heavy-Ion, Hadron, Spin and Astroparticle Studies*, [1807.00603](#).
- [19] U. D’Alesio, F. Murgia, C. Pisano and P. Tael, *Azimuthal asymmetries in semi-inclusive J/ψ + jet production at an EIC*, *Phys. Rev. D* **100** (2019) 094016, [[1908.00446](#)].

- [20] M. G. Echevarria, *Proper TMD factorization for quarkonia production: $pp \rightarrow \eta_{c,b}$ as a study case*, *JHEP* **10** (2019) 144, [[1907.06494](#)].
- [21] S. Fleming, Y. Makris and T. Mehen, *An effective field theory approach to quarkonium at small transverse momentum*, *JHEP* **04** (2020) 122, [[1910.03586](#)].
- [22] F. Scarpa, D. Boer, M. G. Echevarria, J.-P. Lansberg, C. Pisano and M. Schlegel, *Studies of gluon TMDs and their evolution using quarkonium-pair production at the LHC*, *Eur. Phys. J. C* **80** (2020) 87, [[1909.05769](#)].
- [23] M. Grewal, Z.-B. Kang, J.-W. Qiu and A. Signori, *Predictive power of transverse-momentum-dependent distributions*, *Phys. Rev. D* **101** (2020) 114023, [[2003.07453](#)].
- [24] D. Boer, U. D’Alesio, F. Murgia, C. Pisano and P. Tael, *J/ψ meson production in SIDIS: matching high and low transverse momentum*, [[2004.06740](#)].
- [25] M. G. Echevarria, Y. Makris and I. Scimemi, *Quarkonium TMD fragmentation functions in NRQCD*, [[2007.05547](#)].
- [26] B. Page, X. Chu and E. Aschenauer, *Experimental Aspects of Jet Physics at a Future EIC*, *Phys. Rev. D* **101** (2020) 072003, [[1911.00657](#)].
- [27] R. Abdul Khalek et al., *Science Requirements and Detector Concepts for the Electron-Ion Collider: EIC Yellow Report*, [[2103.05419](#)].
- [28] R. F. del Castillo, M. G. Echevarria, Y. Makris and I. Scimemi, *TMD factorization for dijet and heavy-meson pair in DIS*, *JHEP* **01** (2021) 088, [[2008.07531](#)].
- [29] F. Dominguez, B.-W. Xiao and F. Yuan, *k_t -factorization for Hard Processes in Nuclei*, *Phys. Rev. Lett.* **106** (2011) 022301, [[1009.2141](#)].
- [30] Y. Hatta, N. Mueller, T. Ueda and F. Yuan, *QCD Resummation in Hard Diffractive Dijet Production at the Electron-Ion Collider*, *Phys. Lett. B* **802** (2020) 135211, [[1907.09491](#)].
- [31] R. Zhu, P. Sun and F. Yuan, *Low Transverse Momentum Heavy Quark Pair Production to Probe Gluon Tomography*, *Phys. Lett. B* **727** (2013) 474–479, [[1309.0780](#)].
- [32] G.-P. Zhang, *Back-to-back heavy quark pair production in Semi-inclusive DIS*, *JHEP* **11** (2017) 069, [[1709.08970](#)].
- [33] D. Boer, S. J. Brodsky, P. J. Mulders and C. Pisano, *Direct Probes of Linearly Polarized Gluons inside Unpolarized Hadrons*, *Phys. Rev. Lett.* **106** (2011) 132001, [[1011.4225](#)].
- [34] M. Arratia, Y. Furltova, T. J. Hobbs, F. Olness and S. J. Sekula, *Charm jets as a probe for strangeness at the future Electron-Ion Collider*, *Phys. Rev. D* **103** (2021) 074023, [[2006.12520](#)].
- [35] E. Chudakov, D. Higinbotham, C. Hyde, S. Furltov, Y. Furltova, D. Nguyen et al., *Heavy quark production at an Electron-Ion Collider*, *J. Phys. Conf. Ser.* **770** (2016) 012042, [[1610.08536](#)].
- [36] H. T. Li, Z. L. Liu and I. Vitev, *Heavy meson tomography of cold nuclear matter at the electron-ion collider*, *Phys. Lett. B* **816** (2021) 136261, [[2007.10994](#)].
- [37] “artemide web-page, <https://teorica.fis.ucm.es/artemide/> artemide repository, <https://github.com/vladimirovalexy/artemide-public>.”
- [38] I. Scimemi and A. Vladimirov, *Non-perturbative structure of semi-inclusive deep-inelastic and Drell-Yan scattering at small transverse momentum*, *JHEP* **06** (2020) 137, [[1912.06532](#)].
- [39] I. Scimemi and A. Vladimirov, *Systematic analysis of double-scale evolution*, *JHEP* **08** (2018) 003, [[1803.11089](#)].

- [40] T. Gehrmann, T. Luebbert and L. L. Yang, *Calculation of the transverse parton distribution functions at next-to-next-to-leading order*, *JHEP* **06** (2014) 155, [[1403.6451](#)].
- [41] M. G. Echevarria, I. Scimemi and A. Vladimirov, *Unpolarized Transverse Momentum Dependent Parton Distribution and Fragmentation Functions at next-to-next-to-leading order*, *JHEP* **09** (2016) 004, [[1604.07869](#)].
- [42] M.-X. Luo, X. Wang, X. Xu, L. L. Yang, T.-Z. Yang and H. X. Zhu, *Transverse Parton Distribution and Fragmentation Functions at NNLO: the Quark Case*, [1908.03831](#).
- [43] M.-X. Luo, T.-Z. Yang, H. X. Zhu and Y. J. Zhu, *Transverse Parton Distribution and Fragmentation Functions at NNLO: the Gluon Case*, *JHEP* **01** (2020) 040, [[1909.13820](#)].
- [44] M.-x. Luo, T.-Z. Yang, H. X. Zhu and Y. J. Zhu, *Quark Transverse Parton Distribution at the Next-to-Next-to-Next-to-Leading Order*, *Phys. Rev. Lett.* **124** (2020) 092001, [[1912.05778](#)].
- [45] M.-x. Luo, T.-Z. Yang, H. X. Zhu and Y. J. Zhu, *Unpolarized quark and gluon TMD PDFs and FFs at N³LO*, *JHEP* **06** (2021) 115, [[2012.03256](#)].
- [46] A. Hornig, Y. Makris and T. Mehen, *Jet Shapes in Dijet Events at the LHC in SCET*, *JHEP* **04** (2016) 097, [[1601.01319](#)].
- [47] M. G. Buffing, Z.-B. Kang, K. Lee and X. Liu, *A transverse momentum dependent framework for back-to-back photon+jet production*, [1812.07549](#).
- [48] T. Becher and M. D. Schwartz, *Direct photon production with effective field theory*, *JHEP* **02** (2010) 040, [[0911.0681](#)].
- [49] T. Becher, C. Lorentzen and M. D. Schwartz, *Precision Direct Photon and W-Boson Spectra at High p_T and Comparison to LHC Data*, *Phys. Rev. D* **86** (2012) 054026, [[1206.6115](#)].
- [50] Y.-T. Chien, R. Rahn, S. Schrijnder van Velzen, D. Y. Shao, W. J. Waalewijn and B. Wu, *Azimuthal angle for boson-jet production in the back-to-back limit*, [2005.12279](#).
- [51] R. Jaffe and L. Randall, *Heavy quark fragmentation into heavy mesons*, *Nucl. Phys. B* **412** (1994) 79–105, [[hep-ph/9306201](#)].
- [52] M. Fickinger, S. Fleming, C. Kim and E. Mereghetti, *Effective field theory approach to heavy quark fragmentation*, *JHEP* **11** (2016) 095, [[1606.07737](#)].
- [53] D. Boer, P. J. Mulders, C. Pisano and J. Zhou, *Asymmetries in Heavy Quark Pair and Dijet Production at an EIC*, *JHEP* **08** (2016) 001, [[1605.07934](#)].
- [54] Z.-B. Kang, K. Lee, D. Y. Shao and J. Terry, *The Sivers Asymmetry in Hadronic Dijet Production*, [2008.05470](#).
- [55] P. Sun, C. P. Yuan and F. Yuan, *Soft Gluon Resummations in Dijet Azimuthal Angular Correlations in Hadronic Collisions*, *Phys. Rev. Lett.* **113** (2014) 232001, [[1405.1105](#)].
- [56] P. Sun, C. P. Yuan and F. Yuan, *Transverse Momentum Resummation for Dijet Correlation in Hadronic Collisions*, *Phys. Rev. D* **92** (2015) 094007, [[1506.06170](#)].
- [57] A. Hornig, Y. Makris and T. Mehen, *Jet shapes in dijet events at the lhc in scet*, *Journal of High Energy Physics* **2016** (Apr, 2016) 1?41.
- [58] J. Collins, *Foundations of perturbative QCD*. Cambridge University Press, 2013.
- [59] M. G. Echevarria, A. Idilbi and I. Scimemi, *Factorization Theorem For Drell-Yan At Low q_T And Transverse Momentum Distributions On-The-Light-Cone*, *JHEP* **07** (2012) 002, [[1111.4996](#)].
- [60] M. G. Echevarria, I. Scimemi and A. Vladimirov, *Universal transverse momentum dependent soft function at NNLO*, *Phys. Rev.* **D93** (2016) 054004, [[1511.05590](#)].